the plant journal

SEB SOCIETY FOR EXPERIMENTAL BIOLOGY

The Plant Journal (2023) doi: 10.1111/tpj.16218

Salicylic acid inhibits rice endocytic protein trafficking mediated by OsPIN3t and clathrin to affect root growth

Lihui Jiang[1,2,3,†], Baolin Yao[4,†], Xiaoyan Zhang[1,2,3,†], Lixia Wu[1,2,3,5,†], Qijing Fu[1,2,3], Yiting Zhao[1,2,3,6], Yuxin Cao[7], Ruomeng Zhu[7], Xinqi Lu[1], Wuying Huang[1], Jianping Zhao[1,2,3], Kuixiu Li[1,2,3], Shuanglu Zhao[1], Li Han[1,2,3], Xuan Zhou[1,2,3], Chongyu Luo[1,2,3], Haiyan Zhu[1,2,3], Jing Yang[1,2,3], Huichuan Huang[1,2,3], Zhengge Zhu[8], Xiahong He[1,2,3], Jiří Friml[9], Zhongkai Zhang[7,*], Changning Liu[4,10,11,*] and Yunlong Du[1,2,3,*]

[1]*College of Plant Protection, Yunnan Agricultural University, Kunming 650201, China,*
[2]*State Key Laboratory for Conservation and Utilization of Bio-Resources in Yunnan, Yunnan Agricultural University, Kunming 650201, China,*
[3]*Key Laboratory of Agro-Biodiversity and Pest Management of Education Ministry of China, Yunnan Agricultural University, Kunming 650201, China,*
[4]*CAS Key Laboratory of Tropical Plant Resources and Sustainable Use, Xishuangbanna Tropical Botanical Garden, Chinese Academy of Sciences, Menglun, Mengla 666303,Yunnan, China,*
[5]*National Engineering Laboratory for Tree Breeding, Beijing Forestry University, Beijing 100083, China,*
[6]*Shanxi Agricultural University/Shanxi Academy of Agricultural Sciences, The Industrial Crop Institute, Fenyang 032200, China,*
[7]*Key Lab of Agricultural Biotechnology of Yunnan Province, Biotechnology and Germplasm Resources Research Institute, Yunnan Academy of Agricultural Sciences, Kunming 650205,Yunnan, China,*
[8]*Ministry of Education Key Laboratory of Molecular and Cellular Biology, Hebei Collaboration Innovation Center for Cell Signaling and Environmental Adaptation, Hebei Key Laboratory of Molecular and Cellular Biology, College of Life Sciences, Hebei Normal University, Shijiazhuang 050024, China,*
[9]*Institute of Science and Technology Austria (IST Austria), Klosterneuburg, Austria,*
[10]*Center of Economic Botany, Core Botanical Gardens, Chinese Academy of Sciences, Menglun, Mengla 666303,Yunnan, China, and*
[11]*The Innovative Academy of Seed Design, Chinese Academy of Sciences, Menglun, Mengla 666303,Yunnan, China*

Received 3 June 2022; revised 21 March 2023; accepted 24 March 2023.
*For correspondence (e-mail yunlongdu@aliyun.com; liuchangning@xtbg.ac.cn; zhongkai99@sina.com).
†These authors are contributed equally to this work.

SUMMARY

Salicylic acid (SA) plays important roles in different aspects of plant development, including root growth, where auxin is also a major player by means of its asymmetric distribution. However, the mechanism underlying the effect of SA on the development of rice roots remains poorly understood. Here, we show that SA inhibits rice root growth by interfering with auxin transport associated with the OsPIN3t- and clathrin-mediated gene regulatory network (GRN). SA inhibits root growth as well as Brefeldin A-sensitive trafficking through a non-canonical SA signaling mechanism. Transcriptome analysis of rice seedlings treated with SA revealed that the OsPIN3t auxin transporter is at the center of a GRN involving the coat protein clathrin. The root growth and endocytic trafficking in both the *pin3t* and clathrin heavy chain mutants were SA insensitivity. SA inhibitory effect on the endocytosis of OsPIN3t was dependent on clathrin; however, the root growth and endocytic trafficking mediated by tyrphostin A23 (TyrA23) were independent of the *pin3t* mutant under SA treatment. These data reveal that SA affects rice root growth through the convergence of transcriptional and non-SA signaling mechanisms involving OsPIN3t-mediated auxin transport and clathrin-mediated trafficking as key components.

Keywords: auxin, clathrin, endocytosis, *Oryza sativa*, OsPIN3t, salicylic acid.

INTRODUCTION

Salicylic acid (SA) is an important phytohormone in plant development. In the dicotyledon *Arabidopsis thaliana*, SA is involved in the regulation of root hair formation (Garcia-Sanchez et al., 2015), root elongation and lateral root initiation (Kim et al., 2012), root waving growth (Zhao et al., 2015) and root meristem patterning (Pasternak et al., 2019). SA affects root growth by broadly regulating the activity of the protein phosphatase 2A complex (Tan et al., 2020). Furthermore, SA functions as a major signal in plant defense, and the SA signaling pathway, including SA receptors NPR1 and NPR3/4, in the plant immune response is clear and well described (Zhou & Zhang, 2020). However, the effect of the SA signaling pathway on rice root development remains unclear.

Endocytosis plays an important role in plant physiology. In plants, the prominent endocytosis regulatory mechanism is dependent on clathrin (Chen et al., 2011). SA can inhibit clathrin-mediated endocytosis (CME) of the auxin efflux transporters, which has an effect on root auxin distribution in *Arabidopsis* (Du et al., 2013; Ke et al., 2021; Wang et al., 2016). Previous literatures demonstrate that SA treatment affects the expression levels of *PIN-FORMED* (*PIN*) genes (Adamowski & Friml, 2015; Armengot et al., 2014; Pasternak et al., 2019). There is evidence that genes of the *PIN* family are critical for polar auxin transport, and can mediate the growth of different plant tissues (Chen et al., 2012; Friml, 2022; Rakusova et al., 2016; Xu et al., 2015). Although there are 13 *PIN* family genes in the rice genome (Li et al., 2019; Wang et al., 2009; Zhang et al., 2012), *OsPIN1a-d*, *OsPIN2*, *OsPIN3t*, *OsPIN5a-c*, *OsPIN8*, *OsPIN9* and *OsPIN10a-b*, only *OsPIN1* (Li et al., 2019; Xu et al., 2005), *OsPIN2* (Chen et al., 2012) and *OsPIN3t* (Zhang et al., 2012) have been characterized, and these have been found to have a function in root development through affecting the polar auxin transport. Furthermore, *OsPIN3t* in particular has been found to be involved in the drought stress response (Zhang et al., 2012). However, the functions of the *OsPIN3t* gene in response to SA treatment and root growth have not been reported to date. We hypothesize that the network relationships between auxin efflux carriers are important for rice root growth.

In this study, we found that SA was able to inhibit endocytosis of the auxin efflux transporter OsPIN3t to disturb auxin transport in rice root growth, leading to SA-induced inhibition of root growth via non-canonical SA signaling. The mechanisms by which SA inhibits root growth and endocytic protein trafficking of rice were dependent both on the OsPIN3t and clathrin. Moreover, when rice roots were treated with SA, the auxin transporter OsPIN3t was found to be in the center of a gene regulatory network (GRN) containing clathrin, with SA inhibiting the CME of OsPIN3t, and the clathrin-mediated root growth and endocytic trafficking were independent of the OsPIN3t. These results provide an insight into the role of SA in the regulation of plant physiological processes mediated by the OsPIN3t and clathrin.

RESULTS

SA modulates auxin-mediated root growth via non-canonical SA signaling

To test the effects of SA on root growth in rice, seedlings of the rice lines LTH (Li Jiang Xin Tuan Hei Gu; Figure 1a, b), which is a paddy rice landrace with high susceptibility to rice blast fungus *Magnaporthe oryzae* (Yang et al., 2022), and the wild-type Nipponbare (Figure 1c,d) were treated with 100 μM SA. Compared with the controls, the primary root length was significantly shorter in both rice lines LTH and Nipponbare after SA treatment (Figure 1g). To investigate this observation genetically, we analyzed the root phenotype of rice line NB-7B-70, which has very high endogenous SA levels (Figure S1a). This rice line NB-7B-70 showed shorter primary roots (Figure 1f,g) compared with the wild-type NB-61-WT (Figure 1e,g).

Figure 1. Salicylic acid (SA) inhibited root growth in rice.
Six-day-old seedlings of rice LTH (a, b), Nipponbare (c, d), NB-61-WT (e) and NB-7B-70 (f) were grown on 1/2 Murashige and Skoog (MS) medium supplemented with 100 μM SA (b, d) or an equivalent volume of dimethylsulfoxide (DMSO) as a control (a, c). Quantification of the length of the primary roots (g) (LTH: $n_{DMSO} = 16$, $n_{SA100} = 21$; NPB: $n_{DMSO} = 30$, $n_{SA100} = 30$; $n_{NB\text{-}61\text{-}WT} = 32$, $n_{NB\text{-}7B\text{-}70} = 36$) shown in images (a–f).
Six-day-old Nipponbare rice seedlings (h, j) were treated with DMSO (h) or 100 μM SA (j), and grown on 1/2 MS medium with 18-h gravity stimulation. Six-day-old seedlings of rice NB-61-WT (i) and NB-7B-70 (k) were grown on 1/2 MS medium with 18-h gravity stimulation. Quantification of root growth angle (l) (NPB: $n_{DMSO} = 35$, $n_{SA100} = 50$; $n_{NB\text{-}61\text{-}WT} = 29$, $n_{NB\text{-}7B\text{-}70} = 30$) shown in images (h–k).
Six-day-old Nipponbare rice seedlings (m, n) were treated with DMSO (m) or 100 μM SA (n) and were grown on 1/2 MS medium with 120-h gravity stimulation. Six-day-old NB-61-WT (o) and NB-7B-70 (p) rice seedlings were grown on 1/2 MS medium with 120-h gravity stimulation. Quantification of the ratio of lateral roots (HR/VR) (q) (NPB: $n_{DMSO} = 36$, $n_{SA100} = 33$; $n_{NB\text{-}61\text{-}WT} = 13$, $n_{NB\text{-}7B\text{-}70} = 17$) shown in images (m–p).
Six-day-old seedlings of rice Nipponbare (r) and *NahG* (s) were grown on 1/2 MS medium. Quantification of the length of the primary roots (t) ($n_{NPB} = 50$, $n_{NahG} = 36$) shown in images (r) and (s). Six-day-old seedlings of rice Nipponbare (u) and *NahG* (v) were grown on 1/2 MS medium with 18-h gravity stimulation. Quantification of root growth angle (w) ($n_{NPB} = 48$, $n_{NahG} = 31$) shown in images (u–v).
Six-day-old seedlings of rice NPB (x) and *NahG* (y) were grown on 1/2 MS medium with 120-h gravity stimulation. Quantification of the ratio of number of lateral roots (HR/VR) (z) ($n_{NPB} = 23$, $n_{NahG} = 16$) shown in images (x) and (y). G, gravity; HR, number of lateral roots growing from the horizontal part of primary root; LTH, Li Jiang Xin Tuan Hei Gu; ND, no difference; NPB, Nipponbare; VR, number of lateral roots growing from the vertical part of primary root. Data are means ± SD; $*P < 0.05$, $**P < 0.01$ (Student's *t*-test). Scale bar: 1 cm. Arrows indicate the direction of gravity.

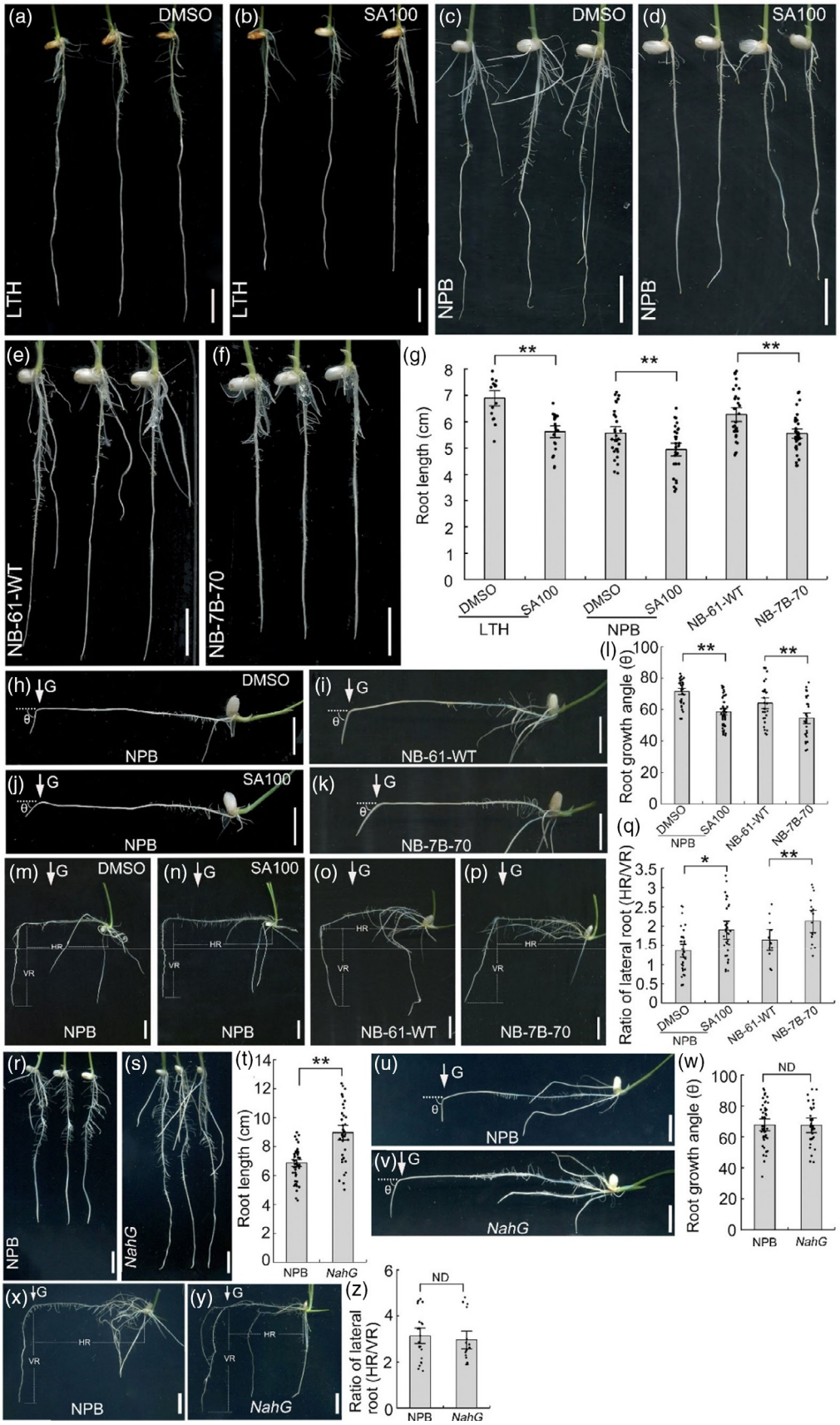

When we investigated the root phenotype of rice line *NahG* (Figure 1s), which has lower levels of SA (Figure S1a), compared with wild-type Nipponbare (Figure 1r), the rice *NahG* had longer roots (Figure 1t). We further found that the root growth rate in the rice lines LTH (Figure S2a–d) and Nipponbare (Figure S2e–h) treated with 100 and 200 μM SA were inhibited, whereas the root growth rate in the rice line *NahG* (Figure S2j,k) was increased compared with the wild-type Nipponbare (Figure S2i).

Next, we tested the effect of SA treatment on rice root gravitropic growth. Compared with the control (Figure 1h, m), Nipponbare seedlings treated with 100 μM SA (Figure 1j,n) showed a smaller root bending angle than the control (Figure 1l), and more lateral roots grown in the horizontal part of the primary root than in the vertical part of the primary root (Figure 1q) grown under gravity stimulation. When rice line NB-7B-70 seedlings (Figure 1k,p) were grown under gravity stimulation, they also showed a smaller root growth angle (Figure 1l) and more lateral roots grown from the horizontal part of the primary root than the vertical part of the primary root (Figure 1q) compared with the wild-type NB-61-WT (Figure 1i,o). When seedlings of rice *NahG* (Figure 1v,y) were grown under gravity stimulation, there were no significant differences in root growth angles (Figure 1w) and the number of lateral roots (Figure 1z) compared with the wild-type Nipponbare (Figure 1u,x).

Next, we tested whether SA affected rice root growth through the established canonical SA signaling pathway (Ding et al., 2018; Wu et al., 2012; Yan & Dong, 2014). In the rice genome, the SA receptor OsNPR1 has a homologous OsNPR3 encoded by the gene *Os03g0667100*. In this study, we used the *OsNPR1*-RNAi line (Yuan et al., 2007), in which the expression level of *OsNPR1* is downregulated (Figure S3), to detect root growth after seedlings were treated with 100 μM SA. It showed that SA treatment inhibited the root lengths of the wild-type rice TP309 (Figure 2b,e) as well as the *OsNPR1*-RNAi line (Figure 2d,e) compared with seedlings treated with dimethylsulfoxide (DMSO) as a control (Figure 2a,c). Compared with the TP309 treated with DMSO (Figure 2a) or 100 μM SA (Figure 2b), the rice line *OsNPR1*-RNAi (Figure 2c,d) showed shorter root lengths (Figure 2e) following either DMSO (Figure 2c) or SA (Figure 2d) treatments. Furthermore, when the TP309 (Figure 2f,g,k,l) and *OsNPR1*-RNAi (Figure 2h,i,m,n) were treated with 100 μM SA (Figure 2g,i,l,n) and grown under gravity stimulation, the seedlings of the wild-type TP309 (Figure 2g,l) and the rice line *OsNPR1*-RNAi (Figure 2i,n) showed smaller root growth angles (Figure 2g,i,j) and a greater ratio of lateral roots (Figure 2l,n,o) compared with seedlings treated with DMSO as a control (Figure 2f,h,k,m). Furthermore, the root growth angles (Figure 2j) and ratio of lateral roots (Figure 2o) did not differ between the wild-type TP309 (Figure 2f,g,k,l) and the *OsNPR1*-RNAi line (Figure 2h,i,m,n) following treatment with either DMSO (Figure 2f,h,k,m) or SA (Figure 2g,i,l,n). We further analyzed the root phenotype of the rice *npr1* mutant, which was created using the CRISPR/Cas9 method (Figure S4a,b), and which has decreased expression levels of *OsNPR1* in the root (Figure S4c). Compared with the seedlings treated with DMSO as control (Figure S5a,c,f,h,k,m), seedlings of rice wild-type Zhonghua 11 (ZH11; Figure S5a,b,f,g,k,l) and the rice *npr1* mutant (Figure S5c,d,h,i,m,n) treated with 100 μM SA (Figure 2b,d,g,i,l,n) also showed shorter root lengths (Figure S5b,d,e), and smaller root growth angles (Figure S5g,i,j) and a higher proportion of lateral roots (Figure S5l,n,o) under gravity stimulation. This suggests that the SA-induced inhibition of root growth is independent of the known canonical SA signaling pathway.

Given that root growth and architecture strongly depend on auxin and its asymmetric distribution (Zhao et al., 2021), we next tested the impact of the SA treatment on auxin levels. We measured auxin levels in the roots of the LTH and Nipponbare lines treated with 100 μM SA after gravity stimulation (Figure S6). The results of this experiment suggest that SA treatment increased the auxin levels in the horizontal part of the primary root (Figure S6b,c). We then checked the auxin levels in the rice lines NB-7B-70 and *NahG* grown under gravity stimulation conditions. Compared with the wild-type NB-61-WT (Figure S6d) and Nipponbare (Figure S6e), the auxin levels in the horizontal part of the primary root of rice NB-7B-70 were increased (Figure S6d), but were decreased in the *NahG* line (Figure S6e). Again, we tested involvement of the canonical SA pathway. Both the seedlings of rice wild-type TP309 and the SA signal mutant *OsNPR1*-RNAi with 100 μM SA treatment under gravity stimulation demonstrated a similar increase in auxin levels in the horizontal part of the primary roots (Figure S6f), and no differences in auxin content between the rice TP309 and *OsNPR1*-RNAi lines treated with either DMSO or 100 μM SA were observed (Figure S6f). These data suggest that the SA-mediated effect on auxin transport and regulating root growth is not mediated by canonical *OsNPR1*-dependent signaling.

SA interferes with Brefeldin A-sensitive endocytic trafficking in rice root epidermal cells

Salicylic acid has been shown to inhibit Brefeldin A (BFA)-sensitive trafficking in *Arabidopsis* (Du et al., 2013; Tan et al., 2020). To test whether SA was able to influence endocytic trafficking of rice root cells to disturb auxin transport in root growth, rice roots were co-treated with SA and the endocytic tracer, the dye FM4-64, which labels plasma membranes and enables visualization of endocytic trafficking (Jelinkova et al., 2010). The result of this experiment showed that the signal intensity on the plasma membrane of root epidermal cells was enhanced following

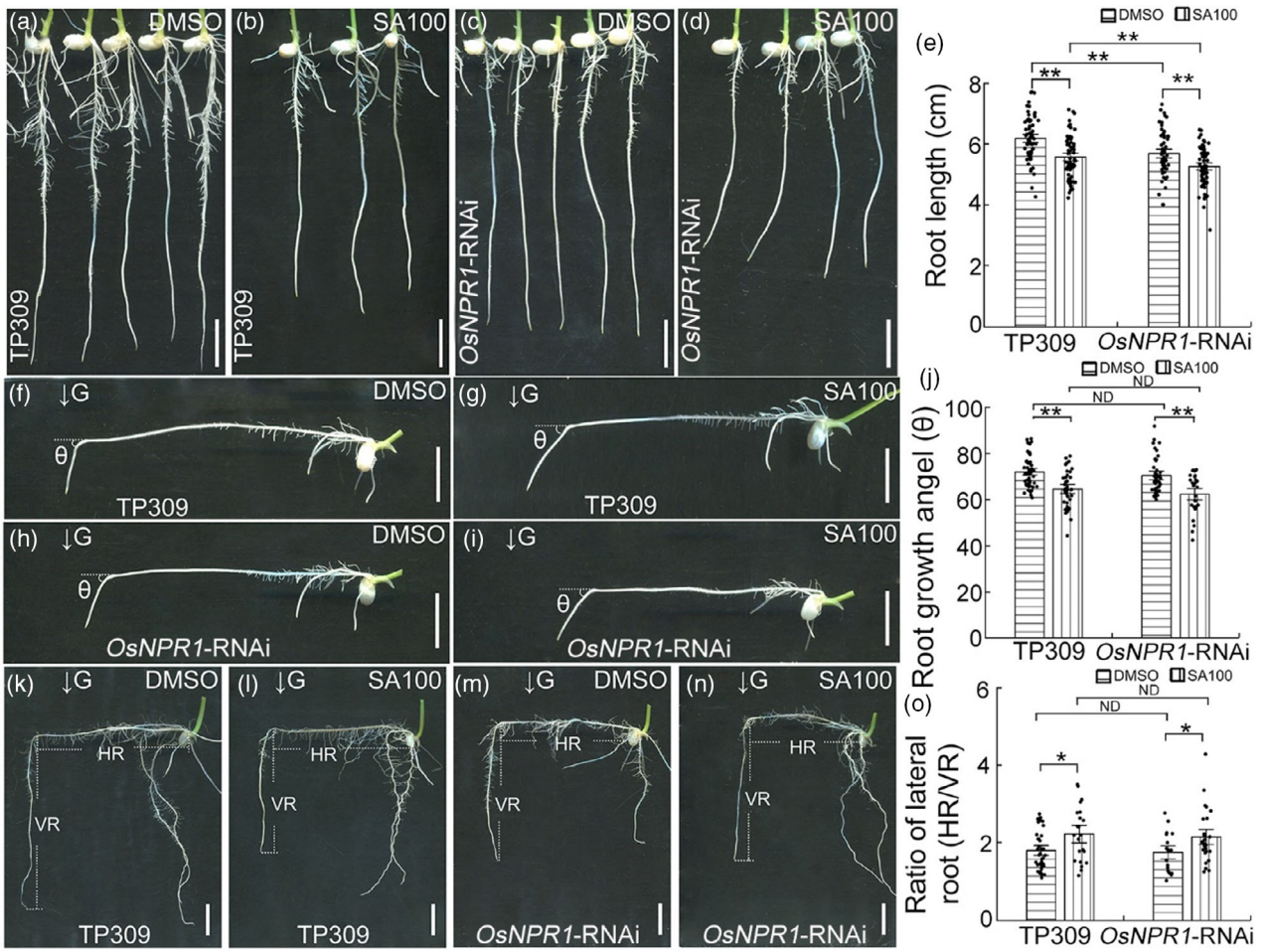

Figure 2. Root phenotype of rice *OsNPR1*-RNAi lines treated with salicylic acid (SA).
Six-day-old seedlings of the rice lines *OsNPR1*-RNAi (c, d) and wild-type TP309 (a, b) were treated with 100 μM SA (b, d), with an equivalent volume of dimethylsulfoxide (DMSO) treatment as a control (a, c). Quantification of the length of the primary roots (e) (TP309: $n_{DMSO} = 65$, $n_{SA100} = 69$; *OsNPR1*-RNAi: $n_{DMSO} = 59$, $n_{SA100} = 66$) shown in images (a–d).
Six-day-old rice seedlings of the lines *OsNPR1*-RNAi (h, i) and wild-type TP309 (f, g) were treated with DMSO (f, h) and 100 μM SA (g, i), and grown on 1/2 Murashige and Skoog (MS) medium with 18-h gravity stimulation. Quantification of the root growth angle (j) (TP309: $n_{DMSO} = 48$, $n_{SA100} = 39$; *OsNPR1*-RNAi: $n_{DMSO} = 41$, $n_{SA100} = 31$) shown in images (f–i).
Six-day-old seedlings of the rice lines *OsNPR1*-RNAi (m, n) and wild-type TP309 (k, l) were treated with DMSO (k, m) or 100 μM SA (l, n), and were grown on 1/2 MS medium with 120-h gravity stimulation. Quantification of the ratio of lateral roots (HR/VR) (o) (TP309: $n_{DMSO} = 35$, $n_{SA100} = 22$; *OsNPR1*-RNAi: $n_{DMSO} = 21$, $n_{SA100} = 27$) shown in images (k–n). HR, number of lateral roots growing from the horizontal part of primary root; VR, number of lateral roots growing from the vertical part of primary root. Data are means ± SD; $*P < 0.05$, $**P < 0.01$ (Student's *t*-test). ND, no difference. Scale bar: 1 cm.

treatment with 100 μM SA for 10 min (Figure S7b,c) and 20 min (Figure 3b,c) compared with the control (Figures 3a and S7a). Nipponbare seedling roots were then further treated with 100 μM SA (Figure 3e) in combination with 25 μM BFA, which is an established protein trafficking inhibitor (Geldner et al., 2001) and is used in the observation of vesicle trafficking in rice (Wu et al., 2015). After the SA treatment (Figure 3e), the size of FM4-64-stained, BFA-induced endomembrane internalization aggregates (BFA bodies) was significantly decreased in the epidermal cells (Figure 3k) as compared with the control (Figure 3d,k).

To further confirm that SA interfered with BFA-sensitive trafficking, seedlings of the rice lines NB-7B-70 (Figure 3g), *NahG* (Figure 3j) and NB-7B-76 (Figure 3h), which also have higher endogenous SA levels (Figure S1b), were treated with 25 μM BFA. Compared with the rice wild-type NB-61-WT (Figure 3f), smaller BFA bodies were observed in NB-7B-70 and NB-7B-76 seedlings (Figure 3g,h,k). However, there were bigger BFA bodies in the rice *NahG* line (Figure 3j,k) compared with the rice wild-type Nipponbare (Figure 3i). This shows that SA interferes with BFA-sensitive trafficking in rice. Next, we tested whether SA treatment has an effect on the localization of auxin export proteins, which are known cargoes of BFA-sensitive trafficking (Adamowski & Friml, 2015), using rice lines expressing *pOsPIN1b :: OsPIN1b-GFP* (Figure 3l,m),

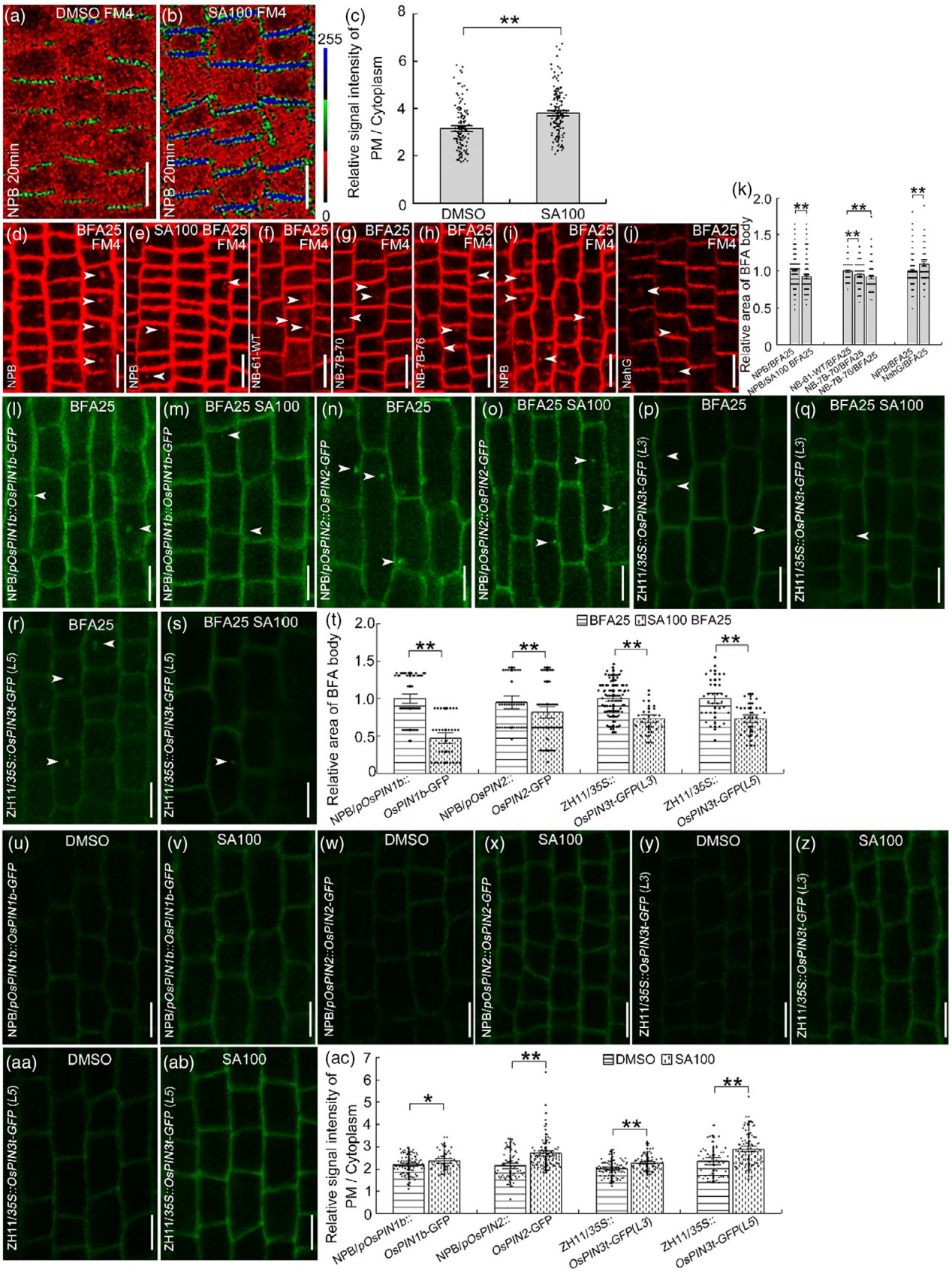

Figure 3. Salicylic acid (SA) treatment inhibited endocytosis of plasma membrane proteins and auxin efflux carriers in rice root epidermal cells.
Root epidermal cells of 6-day-old Nipponbare seedlings were treated with 4 μM FM4-64 plus either 100 μM SA (b) or an equivalent volume of dimethylsulfoxide (DMSO) as a control (a) for 20 min. Quantification of relative fluorescence intensities of plasma membrane versus cytoplasm in rice root epidermal cells (c) (NPB: $n_{DMSO} = 139$, $n_{SA100} = 162$). The roots of 6-day-old Nipponbare seedlings were treated with 4 μM FM4-64 plus either 25 μM Brefeldin A (BFA) for 90 min (d) or cotreated with 100 μM SA (e).
The roots of 6-day-old seedlings of the rice lines NB-7B-70 (g), NB-7B-76 (h) and wild-type NB-61-WT (f), *NahG* (j) and wild-type Nipponbare (i) were treated with 4 μM FM4-64 plus 25 μM BFA for 90 min. Quantification of the relative area of the BFA bodies (k) (NPB: $n_{BFA25} = 733$, $n_{SA100} = 202$; $n_{NB\text{-}61\text{-}WT} = 140$, $n_{NB\text{-}7B\text{-}70} = 250$, $n_{NB\text{-}7B\text{-}76} = 143$; $n_{NPB} = 279$, $n_{NahG} = 117$) shown in images (d–j).
Roots of 14-day-old rice lines expressing *pOsPIN1b :: OsPIN1b-GFP* (l, m), *pOsPIN2 :: OsPIN2-GFP* (n, o) and *35S :: OsPIN3t-GFP* (p–s) were treated with 25 μM BFA for 90 min (l, n, p, r) or cotreated with 100 μM SA (m, o, q, s). Quantification of the relative area of the internalized PIN1-GFP, PIN2-GFP and PIN3t-GFP proteins (t) (NPB/*pOsPIN1b* :: Os*PIN1b-GFP*: $n_{BFA25} = 47$, $n_{SA100} = 43$; NPB/*pOsPIN2 :: OsPIN2-GFP*: $n_{BFA25} = 47$, $n_{SA100} = 60$; ZH11/*35S :: OsPIN3t-GFP*(*L3*): $n_{BFA25} = 102$, $n_{SA100} = 25$; ZH11/*35S :: OsPIN3t-GFP* (*L5*): $n_{BFA25} = 38$, $n_{SA100} = 32$) shown in images (l–s).
Root epidermal cells of 14-day-old rice lines expressing *pOsPIN1b :: OsPIN1b-GFP* (u, v), *pOsPIN2 :: OsPIN2-GFP* (w, x) and *35S :: OsPIN3t-GFP* (y, z, aa, ab) were treated with either 100 μM SA (v, x, z, ab) or equivalent volume of DMSO acted as a control (u, w, y, aa) for 20 min. Quantification of relative fluorescence intensity of plasma membrane versus cytoplasm in rice root epidermal cells (ac) (NPB/*pOsPIN1b* :: Os*PIN1b-GFP*: $n_{DMSO} = 87$, $n_{SA100} = 51$; NPB/*pOsPIN2 :: OsPIN2-GFP*: $n_{DMSO} = 65$, $n_{SA100} = 88$; ZH11/*35S :: OsPIN3t-GFP*(*L3*): $n_{DMSO} = 84$, $n_{SA100} = 74$; ZH11/*35S :: OsPIN3t-GFP* (*L5*): $n_{DMSO} = 52$, $n_{SA100} = 84$) shown in images (u–ab). The relative fluorescence intensity is color-coded: red, low; green, medium; and blue, high fluorescence. Arrow heads indicate the internalization of plasma membrane protein. FM4, FM4-64; NPB, Nipponbare; ZH11, Zhonghua 11. Data are means ± SD; $*P < 0.05$, $**P < 0.01$ (Student's *t*-test). PM, plasma membrane. Scale bar: 10 μm.

pOsPIN2 :: OsPIN2-GFP (Figure 3n,o) and *35S :: OsPIN3t-GFP* (Figure 3p–s). The OsPIN1b, OsPIN2 and OsPIN3t did not show obvious polar localization in the rice root epidermal cells (Figure 3l,n,p,r), in contrast from results of *Arabidopsis* (Adamowski & Friml, 2015; Friml, 2022; Friml et al., 2002), When we analyzed the amino acid sequences of OsPIN1b, OsPIN2 and OsPIN3t, we found that they shared 67.72, 58.54 and 58.11% identities with *Arabidopsis* PIN1, PIN2 and PIN3, respectively. Moreover, the OsPIN1b, OsPIN2 and OsPIN3t contain different membrane transport domains than their *Arabidopsis* homologous PIN1, PIN2 and PIN3, respectively (Figure S8; Additional File S1). Therefore, the different subcellular localization of auxin transporters observed in rice and *Arabidopsis* may result from the sequence differences in the auxin transporters. However, SA treatment inhibited the BFA-induced intracellular aggregation of OsPIN1b (Figure 3m,t), OsPIN2 (Figure 3o,t) and OsPIN3t (Figure 3q,s,t) compared with the controls (Figure 3l,n,p,r). We then checked the subcellular localization of OsPIN1b, OsPIN2 and OsPIN3t following SA treatment. The results of this experiment showed that the signal intensities of OsPIN1b (Figure 3v), OsPIN2 (Figure 3x) and OsPIN3t (Figure 3z,ab) on the plasma membrane were enhanced after 100 μM SA treatment for 20 min (Figure 3ac) as compared with the control (Figure 3u,w,y,aa,ac). These data show that SA may inhibit BFA-sensitive trafficking of endomembranes in general and PIN auxin transporters specifically in rice root epidermal cells, which then affects auxin transport and rice root growth. Ultrastructural observation of BFA compartments did not reveal differences in ultrastructure between BFA and SA/BFA treatments, and the BFA bodies could still be observed in the rice root epidermal cells treated with SA using electron microscopy (Figure 4a–c). We also found that SA treatment did not cause obvious changes in the ultrastructure of organelle and vesicle compartments (Figure S9).

Non-canonical SA signaling is involved in BFA-sensitive trafficking

To gain insight into the mechanism underlying the effect of SA on BFA-sensitive trafficking in rice, we treated Nipponbare seedling roots with BFA and SA, accompanied by an inhibitor of protein synthesis (cycloheximide, CHX; Figure 4d,e) and the proteasome inhibitor MG132 (carbobenzoxy-L-leucyl-L-leucyl-L-leucine; Figure S7d,e). Under these conditions, SA treatment was also found to inhibit formation of the BFA bodies (Figures 4e,j and S7e,f) compared with the control (Figures 4d and S7d). To test whether canonical SA signaling is required for the effect on trafficking, we used the rice line *OsNPR1*-RNAi, and treated it with both SA and BFA (Figure 4i). We found that SA treatment significantly interfered with the formation of BFA bodies in both the wild-type TP309 (Figure 4g,j) and the rice line *OsNPR1*-RNAi (Figure 4i,j) compared with the control (Figure 4f,h). This suggests that the canonical OsNPR1 receptor is not required for the observed effect of SA on BFA-sensitive trafficking.

Transcript analysis of rice LTH root treated with SA

Although we found that the effect of SA on BFA-insensitive trafficking was independent of SA signaling, it is likely that the more complex effect on root growth also has a transcriptional component. To gain insight into the transcriptional component of the mechanism, we analyzed the effect of SA treatment on the rice LTH root transcriptome. The correlation assessment showed that except for the SA-treated sample L-S1, there were strong correlations within biological replicates, including DMSO-treated L-D1, L-D2 and L-D3 (controls), and SA-treated L-S2 and L-S3 (Figure S10a). The subsequent transcriptome analysis was therefore based on the data from these five samples. In the rice roots treated with SA or DMSO, a total of 40.2 Gb clean reads were mapped and assembled into 57 402 unigenes,

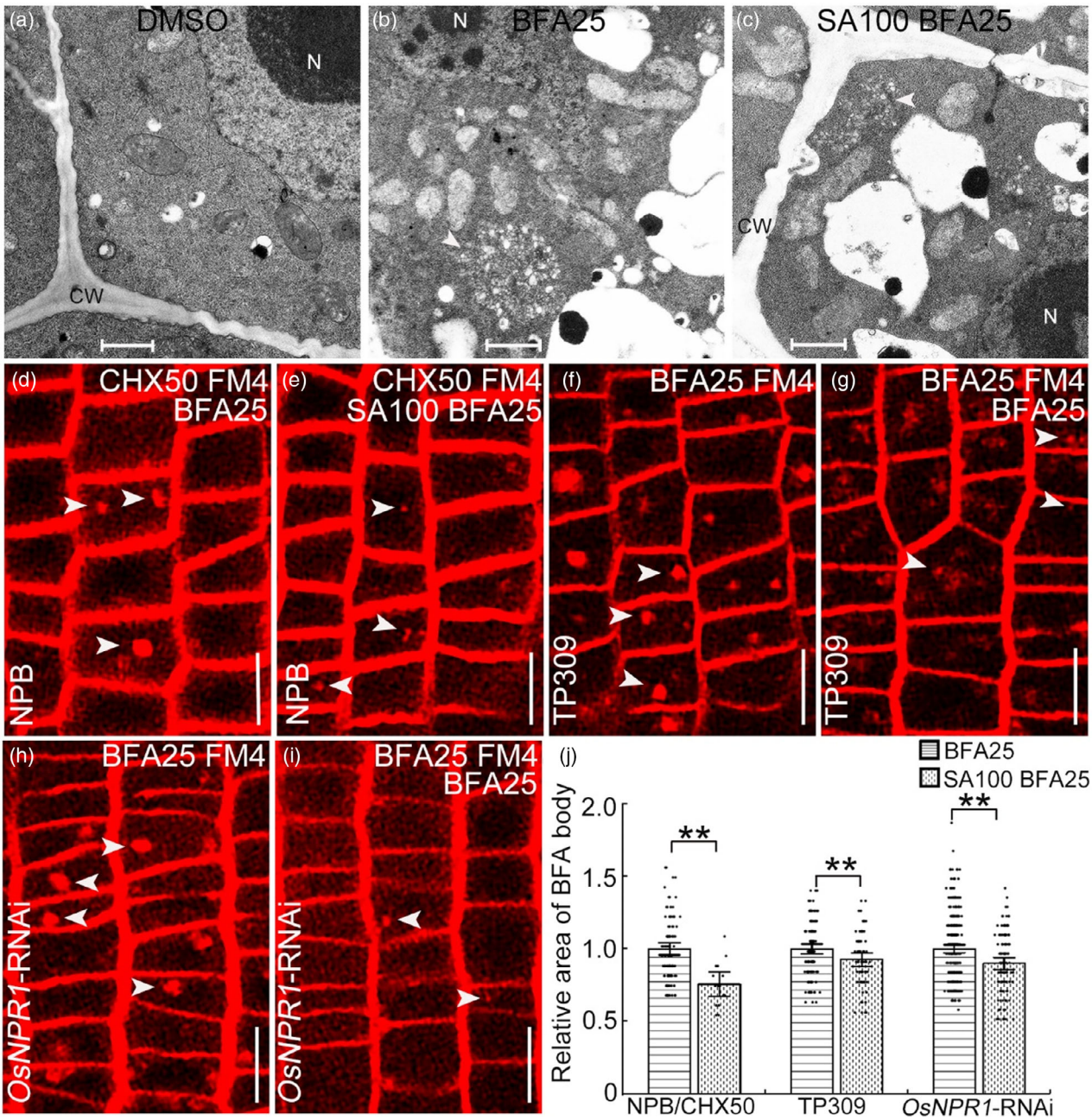

Figure 4. Salicylic acid (SA) inhibition of endocytosis in rice epidermal cells did not disturb the ultrastructure of Brefeldin A (BFA) compartments, and is independent of protein translation and SA signaling pathways.

Roots of 6-day-old rice line NPB seedlings were treated with dimethylsulfoxide (DMSO; acting as a control) (a), and 25 μM Brefeldin A (BFA) (b) or cotreated with 100 μM SA (c) to observe the ultrastructure of BFA bodies.

Roots of 6-day-old Nipponbare seedlings were treated with 4 μM FM4-64 plus either 25 μM BFA and 50 μM cycloheximide (CHX) (d) or cotreated with 100 μM SA (e) for 90 min.

Roots of 6-day-old rice wild-type TP309 (f, g) and *OsNPR1*-RNAi (h, i) seedlings were treated with 4 μM FM4-64 plus either 25 μM BFA (f, h) or cotreated with 100 μM SA (g, i) for 90 min.

Quantification of the relative area of the BFA bodies (j) (Nipponbare: $n_{BFA25} = 103$, $n_{SA100} = 14$; TP309: $n_{BFA25} = 125$, $n_{SA100} = 66$; *OsNPR1*-RNAi: $n_{BFA25} = 290$, $n_{SA100} = 114$) shown in images (d–i). Arrow heads indicate the BFA bodies. CW, cell wall; FM4, FM4-64; N, Nucleus; NPB, Nipponbare. Scale bar: 1 μm (a–c); 10 μm (d–i). Data are means ± SD; $^{**}P < 0.01$ (Student's *t*-test).

including 1146 unannotated transcripts (Additional Files S2 and S3). A total of 56 437 unigenes were annotated against the COG, GO, KEGG, KOG, Pfam, Swiss-prot, eggNOG and NR databases (Figure S10b). The GO assignments could be further divided into three categories, 'cellular component', 'molecular function' and 'biological process' (Figure S10c).

Compared with the DMSO treatment, 1647 differentially expressed genes (DEGs) were detected when seedlings were treated with SA, including 625 (37.95%) upregulated genes and 1022 (62.05%) downregulated genes (Additional File S4). Of the 1647 DEGs, 129 DEGs were associated with transport, synthesis or signal transduction of auxin, 40 DEGs were identified as being involved in endocytosis, and 269 DEGs were identified as being involved in root development (Additional File S5).

The top enriched GO terms of the upregulated DEGs (Figure S11a; Additional File S6) included 'glutathione metabolic process', 'toxin catabolic process', '6-phosphofructokinase complex', 'extracellular matrix', 'glutathione binding' and 'L-amino acid efflux transmembrane transporter activity'. On the other hand, the top enriched GO terms of the downregulated DEGs (Figure S11b; Additional File S7) included 'RNA processing', 'isopentenyl diphosphate biosynthetic process', 'plastoglobule', 'photosystem II', 'chlorophyll binding' and 'poly (U) RNA binding'.

Intriguingly, in the KEGG pathway enrichment analysis of the upregulated DEGs (Figure S12a), the most significant pathway was found to be 'glutathione metabolism', which was consistent with the GO term 'glutathione metabolic process'. In the KEGG pathway enrichment analysis of the downregulated DEGs (Figure S12b), the most significant pathways were found to be 'photosynthesis – antenna proteins' and 'photosynthesis', indicating that the downregulated DEGs were relevant to the metabolism of photosynthesis, which was also consistent with the GO terms 'photosystem II' and 'chloroplast thylakoid lumen' in the GO enrichment analysis (Figure S11b; Additional File S7).

We randomly selected 25 DEGs and validated their expression levels using quantitative reverse transcriptase-polymerase chain reaction (qRT-PCR). The qRT-PCR results showed that the expression trends of these DEGs (Figure S13b) were consistent with those of the transcriptome sequencing (Figure S13a), and all showed significant differential expression, which also supports the reliability of the high-throughput RNA sequencing data.

Network analysis of DEGs reveals an *OsPIN3t*-centered GRN

To further explore the regulatory networks in which the DEGs may participate, a rice SA related GRN was constructed by combining the known regulatory relationship pairs from RiceNetDB (Lee et al., 2011; Liu et al., 2013). A total of 6606 genes, including 5801 non-DEGs and 805 DEGs, were aligned to the RiceNetDB database (Figure S14; Additional File S8). We then examined the hub genes in the network, with the results suggesting that there were 30 hub genes in total (Additional File S9).

In this rice SA-related GRN, we found one DEG, *OsPIN3t* (Os01g45550), coding for the PIN auxin exporter, which further regulated 10 downstream genes (Figure S14). However, we found no DEGs regulating *OsPIN3t* upstream. We wanted to gain clues as to the mechanism underlying the involvement of the *OsPIN3t* gene in the SA regulation of root growth, and we therefore constructed a sub-GRN between *OsPIN3t*, its 10 downstream genes and the genes associated with these downstream genes (Figure 5a). This sub-GRN suggested that *OsPIN3t* could directly or indirectly interact with several different genes, including *OsPIN1a* (Li et al., 2019), *OsPIN2* (Chen et al., 2012; Inahashi et al., 2018; Sun et al., 2019; Wang et al., 2018), *OsPIN5a* (Wang et al., 2009), *ZFP350* (Kang et al., 2019), *SLG* (Feng et al., 2016), *REL2* (Yang et al., 2016), *PME31*(Yang et al., 2013) and *RBG1* (Liu et al., 2015), which are involved in the development of inflorescences, roots, shoots, panicles, tillers, grains and leaves. We further detected the expression levels of *OsPIN3t* in the rice lines NB-7B-70 and *NahG*, which have higher and lower endogenous SA levels, respectively (Figure S1), and found that the *OsPIN3t* levels were downregulated in the rice line NB-7B-70 and upregulated in the rice line *NahG* (Figure S15). It suggests that function of *OsPIN3t* is involved in the SA regulation of rice root growth.

OsPIN3t is involved in SA-mediated rice root growth through the regulation of auxin transport

Interestingly, when we analyzed gene expression levels from the *OsPIN3t* regulatory network, including *OsPIN1a* (Os06g12610), *OsPIN2* (Os06g44970) and *OsPIN5* (Os01g69070), using qRT-PCR, we detected a differential effect of SA on the transcription of these genes in the rice wild-type ZH11 and *pin3t* mutant (Figure S16) compared with the controls (Figure 5b).

Next, we tested the root phenotype of the *pin3t* mutant treated with 100 and 200 μM SA. This analysis revealed that the root length (Figure 6a–g) and root growth rate (Figure S17) were not inhibited in the *pin3t* mutant (Figures 6d–g and S17d–g) compared with the wild-type ZH11 (Figures 6a–c,g and S17a–c,g). The rice *pin3t* mutant also showed no root bending sensitivity to SA following gravity stimulation (Figure 6i,k,l) compared with the wild-type ZH11 (Figure 6h,j,l). Because the root growth in the *pin3t* mutant was SA insensitive, we next tested whether the *pin3t* mutant was involved in the mechanism underlying SA regulation of auxin homeostasis. The wild-type rice line ZH11 (Figure 6h,j) and the *pin3t* mutant (Figure 6i,k) were treated with SA and grown under gravity stimulation. This *pin3t* mutant was insensitive to SA in terms of regulation of indole acetic acid (IAA) levels, as compared with the control (Figure 6m). We further checked the root phenotype under SA treatment of the rice *OsPIN3t*-RNAi line L7, which had lower expression levels of *OsPIN3t* in the root (Figure S18). Both the root lengths (Figure S19d–g)

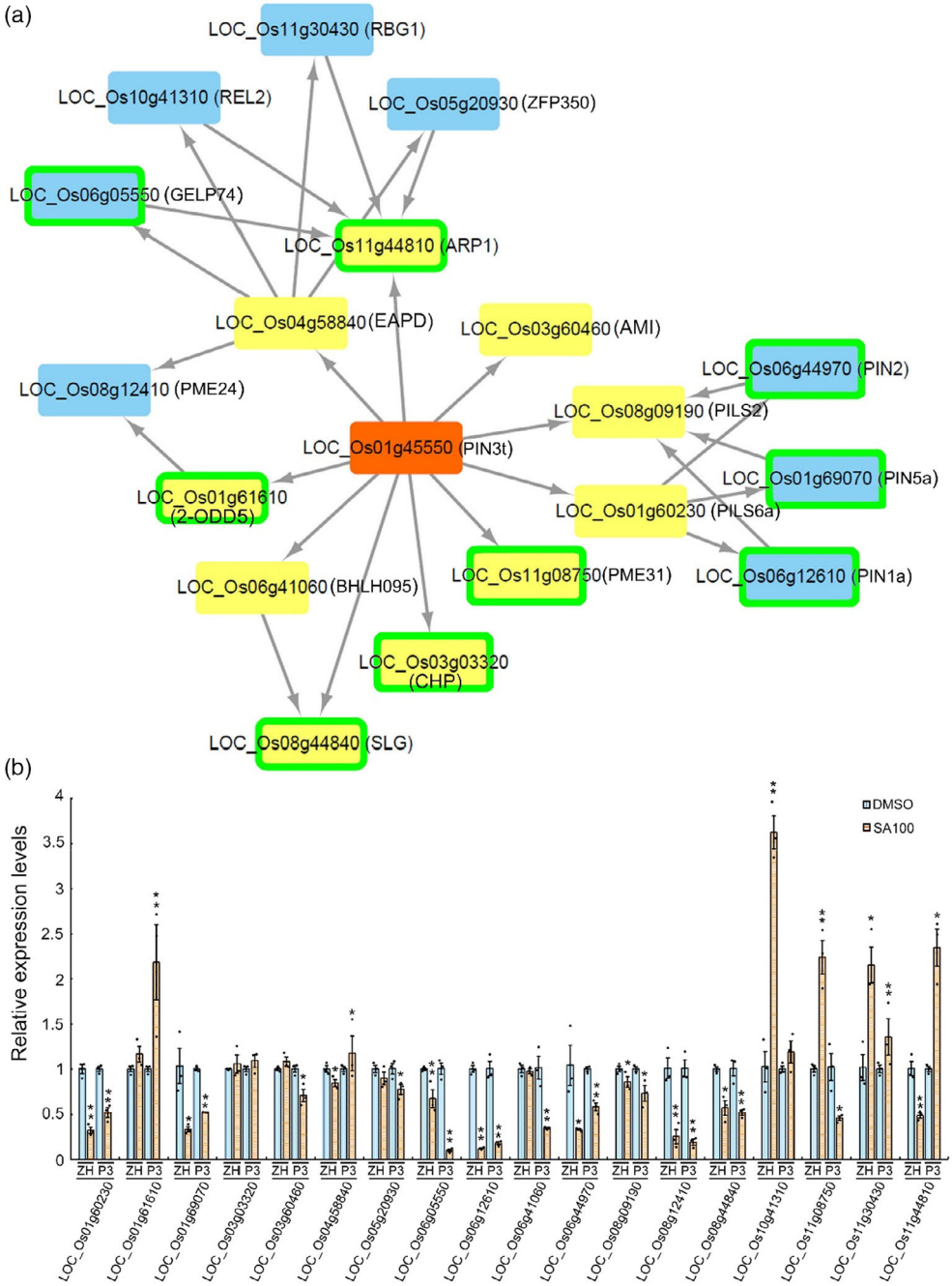

Figure 5. Regulation network of *OsPIN3t* and polymerase chain reaction (PCR) detection.
Regulation network of *OsPIN3t* (a), its 10 downstream genes, and genes associated with them, extracted from the salicylic acid (SA)-related gene regulatory network (GRN) of rice (Figure S13). Light yellow blocks indicate that the gene in the block is regulated directly by *OsPIN3t*. Blue blocks indicate that the gene is indirectly regulated by *OsPIN3t*. Highlighted blocks indicate that the gene in the block is expressed differentially following treatment with SA. Relative expression of genes shown in part (a) from the primary roots of the rice line Zhonghua11 and the *pin3t* mutant following treatment with 100 μM SA or dimethylsulfoxide (DMSO; acting as a control) were determined using quantitative reverse transcriptase (qRT)-PCR (b). The *OsActin* gene was used as an internal control. The data presented here represent at least three biological replicates. Data are means ± SD. $*P < 0.05$, $**P < 0.01$ (SPSS analysis). 2-ODD5, 2-oxoglutarate-dependent dioxygenase 5; AMI, aminopeptidase; ARP1, auxin repressed protein 1; BHLH095, basic helix–loop–helix protein 095; CHP, conserved hypothetical protein; EAPD, eukaryotic aspartyl protease domain; GELP74, GDSL esterase/lipase protein 74; P3, rice *pin3t* mutant; PILS2, PIN likes 2; PILS6a, PIN likes 6a; PIN3t, PIN protein 3a; PIN5a, PIN protein 5a; PIN1a, PIN protein 1a; PIN2, PIN protein 2; PME24, pectin methylesterase 24; PME31, pectin methylesterase 31; REL2, rolled and erect leaf 2; RBG1, rice big grain 1; SLG, slender grain; ZFP350, zinc finger protein 350; ZH, rice Zhonghua 11.

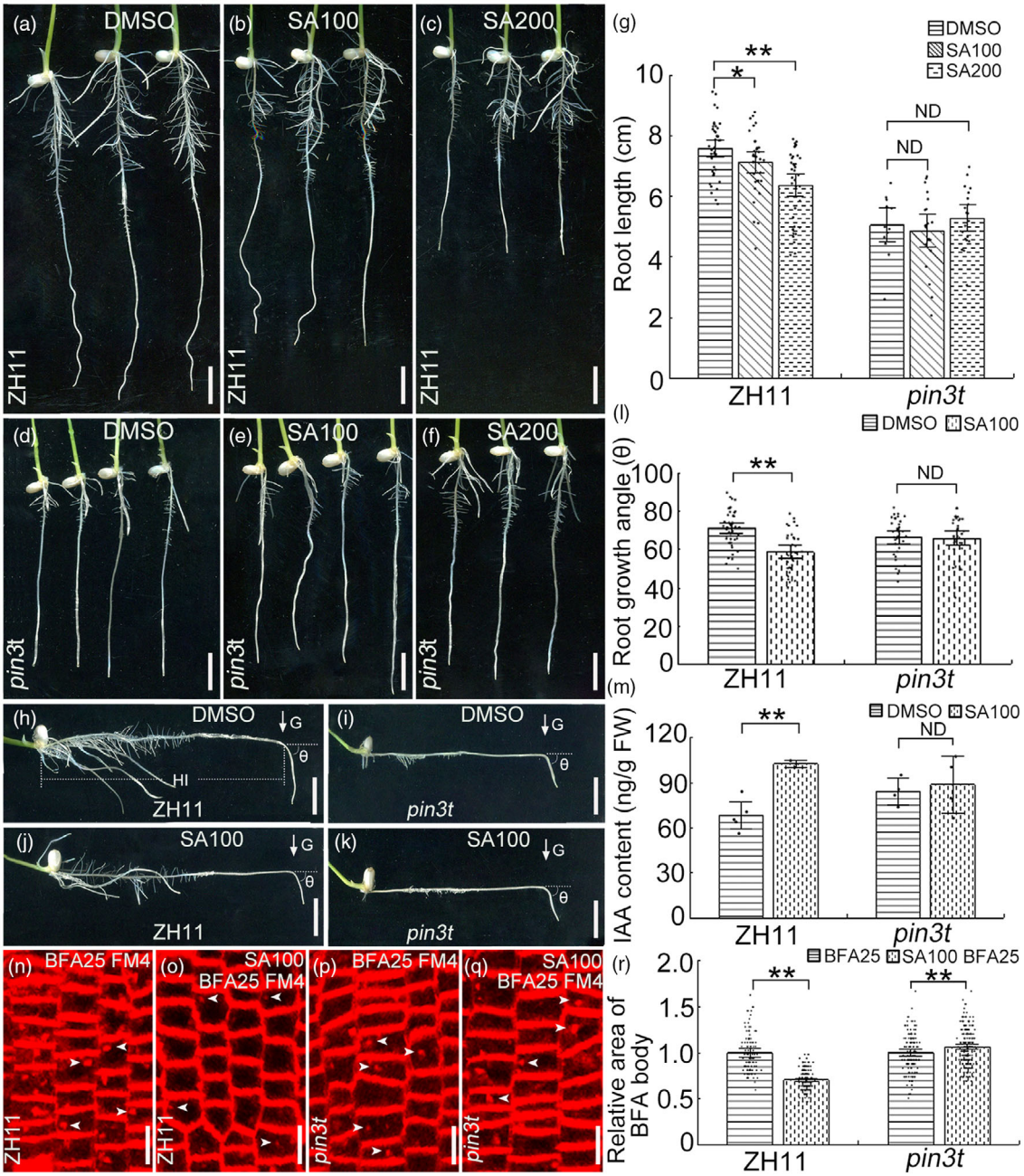

Figure 6. Root phenotype and endocytosis of root epidermal cells in the rice *pin3t* mutant were insensitive to salicylic acid (SA) treatment.
Six-day-old seedlings of the rice lines Zhonghua 11 (a–c) and *pin3t* (d–f) were grown on 1/2 Murashige and Skoog (MS) medium complemented with either 100 μM SA (b, e), 200 μM SA (c, f), or with an equivalent volume of dimethylsulfoxide (DMSO) (a, d) as a control. The primary root length was measured and quantified (g) (Zhonghua 11: $n_{DMSO} = 43$, $n_{SA100} = 35$, $n_{SA200} = 40$; *pin3t*: $n_{DMSO} = 19$, $n_{SA100} = 21$, $n_{SA200} = 20$) shown in images (a–f).
Six-day-old Zhonghua 11 (h, j) and *pin3t* (i, k) seedlings were treated with DMSO (h, i) or 100 μM SA (j, k), and grown on 1/2 MS medium with 18-h gravity stimulation. Quantification of the growth angle (l) (Zhonghua 11: $n_{DMSO} = 45$, $n_{SA100} = 37$; *pin3t*: $n_{DMSO} = 36$, $n_{SA100} = 34$) of the roots shown in images (h–k).
Indole acetic acid (IAA) content (m) (Zhonghua 11: $n_{DMSO} = 5$, $n_{SA100} = 3$; *pin3t*: $n_{DMSO} = 4$, $n_{SA100} = 4$) in the horizontal part of primary roots of rice seedlings treated with 100 μM SA. The roots of 6-day-old seedlings of rice lines Zhonghua 11 (n, o) and *pin3t* mutant (p, q) were treated with 4 μM FM4-64 plus either 25 μM Brefeldin A (BFA) for 90 min (n, p) or with 4 μM FM4-64, 25 μM BFA and 100 μM SA (o, q). Quantification of the relative area of the BFA bodies (r) (Zhonghua 11: $n_{BFA25} = 98$, $n_{SA100BFA25} = 149$, *pin3t*: $n_{BFA25} = 137$, $n_{SA100BFA25} = 216$) shown in images (n–q). Data are means ± SD; $*P < 0.05$, $**P < 0.01$ (Student's *t*-test). G, gravity; ND, no difference; HI, IAA content in the horizontal part of the primary root; ZH11, Zhonghua 11. Arrows indicate the direction of gravity. Arrow heads indicate the BFA bodies. Scale bar: 1 cm (a–c, d–f, h–k); 10 μm (n–q).

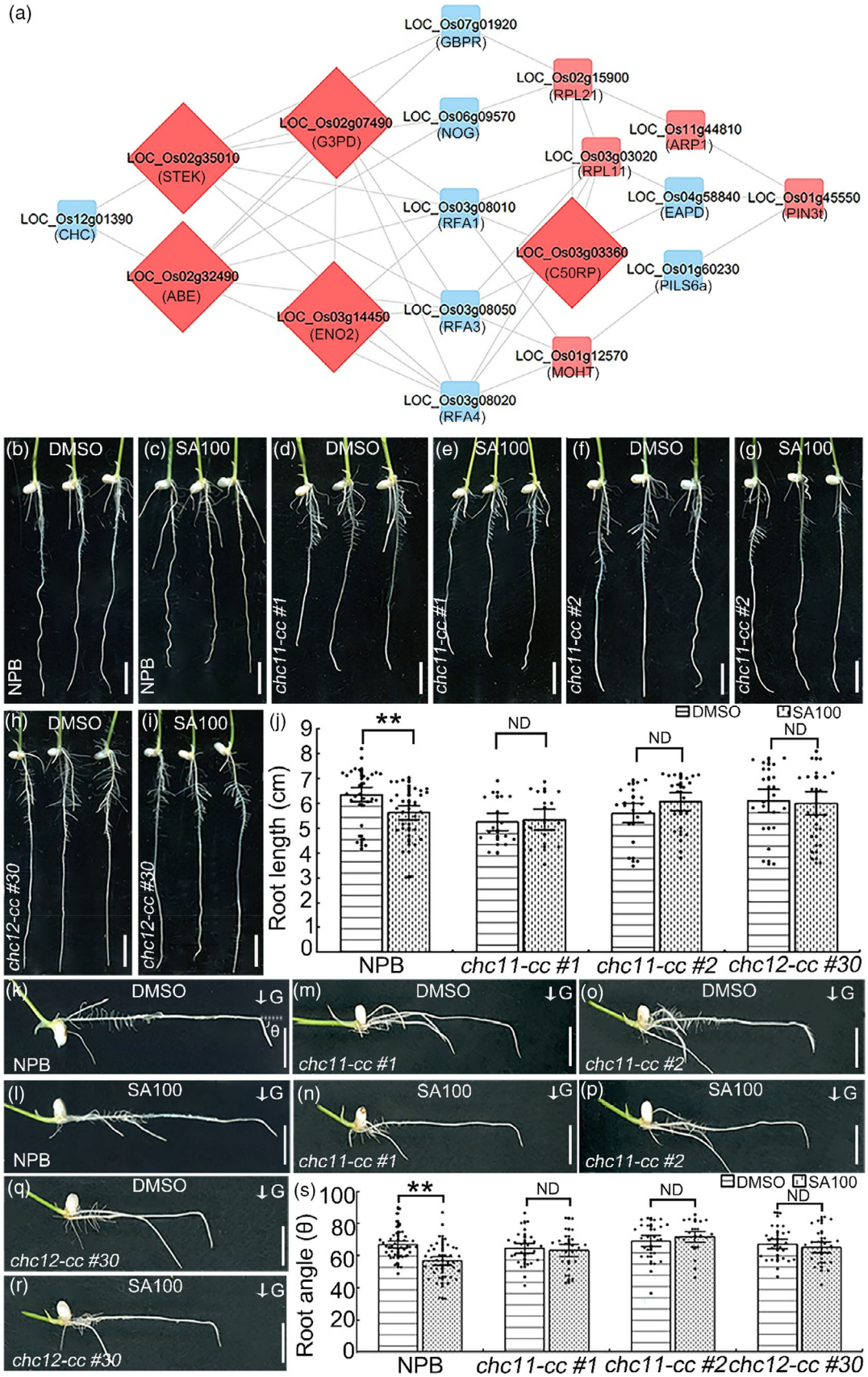

Figure 7. Regulation network of the clathrin gene *Os12g01390* and root phenotypes of the rice clathrin heavy chain (CHC) mutants treated with salicylic acid (SA).
The regulatory network connecting *OsPIN3t* and the CHC encoding gene *Os12g01390* were extracted from the SA-related gene regulatory network (GRN) for rice (Figure S13). Blue blocks indicate that the gene in the block was not found to be differentially expressed in the transcriptome analysis (a). Red blocks indicate that the gene in the block was differentially expressed in the transcriptome analysis (a). The larger blocks indicate hub genes in the regulatory gene network (a).
Six-day-old seedlings of the rice lines Nipponbare (b, c) and *chc11-cc* lines #1 (d, e), #2 (f, g) and *chc12-cc* line #30 (h, i) were grown on 1/2 Murashige and Skoog (MS) medium supplemented with either 100 μM SA (c, e, g, i) or with an equivalent volume of dimethylsulfoxide (DMSO) (b, d, f, h) as a control. The primary root length was measured and quantified (j) (NPB: $n_{DMSO} = 30$, $n_{SA100} = 33$; *chc11-cc* #1: $n_{DMSO} = 16$, $n_{SA100} = 14$, *chc11-cc* #2: $n_{DMSO} = 18$, $n_{SA100} = 22$, *chc12-cc* #30: $n_{DMSO} = 19$, $n_{SA100} = 21$) shown in images (b–i).
Six-day-old seedlings of rice Nipponbare (k, l) and *chc11-cc* lines #1 (m, n), #2 (o, p), and *chc12-cc* line #30 (q, r) were treated with either 100 μM SA (l, n, p, r) or an equivalent volume of DMSO (k, m, o, q), and grown on 1/2 MS medium with 18-h gravity stimulation. Quantification of the growth angle of the roots (s) (NPB: $n_{DMSO} = 30$, $n_{SA100} = 22$; *chc11-cc* #1: $n_{DMSO} = 26$, $n_{SA100} = 22$, *chc11-cc* #2: $n_{DMSO} = 25$, $n_{SA100} = 20$, *chc12-cc* #30: $n_{DMSO} = 27$, $n_{SA100} = 24$) shown in images (k–r). ABE, AMP-binding enzyme; ARP1, auxin repressed protein 1; C50RP, chloroplast 50S ribosomal protein; CHC, clathrin heavy chain; EAPD, eukaryotic aspartyl protease domain; G3PD, glyceraldehyde-3-phosphate dehydrogenase; GBPR, GTP-binding protein-related; ENO2, enolase 2; MOHT, 3-methyl-2-oxobutanoate hydroxymethyltransferase; NOG, nucleolar GTP-binding protein 1; PILS6a, PIN likes 6a, PIN3t, PIN protein 3a; RFA1, rice elongation factor 1A-1; RFA3, rice elongation factor 1A-3; RFA4, rice elongation factor 1A-4; RPL11, 50S ribosomal protein L11; RPL21, 50S ribosomal protein L21; STEK, STE kinase. Scale bar: 1 cm (b–i, k–r). NPB, Nipponbare. Data are means ± SD; $^{**}P < 0.01$ (Student's *t*-test). G, gravity; ND, no difference. Arrows indicate the direction of gravity (k–r).

and root growth angles (Figure S19j–l) of the rice *OsPIN3t*-RNAi line L7 were insensitive to SA treatment compared with the wild-type ZH11 (Figure S19a–c,h–i). Next, we further detected the effect of SA inhibition of endocytic trafficking on the *pin3t* mutant. The roots of the wild-type rice ZH11 (Figure 6n,o) and the *pin3t* mutant (Figure 6p,q) were co-treated with 100 μM SA, 25 μM BFA and 4 μM FM4-64. It showed that SA treatment inhibited the endocytic trafficking of the wild-type rice ZH11 (Figure 6o,r) compared with the control treated with DMSO (Figure 6n); however, the *pin3t* mutant was insensitive to the SA treatment and bigger BFA bodies (Figure 6q) than the control (Figure 6p) were observed in the *pin3t* mutant (Figure 6r). These data suggest that *OsPIN3t* is a key component of the SA signaling network that modulates auxin transport and homeostasis in rice root growth.

Clathrin heavy chain (CHC) mutants are insensitive to SA treatment

It has been reported that CME is targeted by SA-related pathways in *Arabidopsis* (Du et al., 2013). In the rice SA-related GRN (Figure S14), we found one rice clathrin gene homolog, *Os12g01390*, encoding for the CHC. Network analysis showed that Os12g01390 was linked to Os01g45550 (*OsPIN3t*) in a sub-GRN by multiple DEGs, including five hub genes (Figure 7a). Notably, although Os12g01390 was not differentially expressed after SA treatment, two differentially expressed hub genes Os02g32490 and Os02g35010 were shown to directly regulate the expression of Os12g01390, Os02g07490 and Os03g14450 in the sub-GRN (Figure 7a). Interestingly, when we analyzed the rice line expressing *35S::OsPIN3t-GFP*, we found that BFA-mediated trafficking of OsPIN3t showed the same sensitivity to SA (Figure 3q,s,t) as did OsPIN1b and OsPIN2 (Figure 3m,o,t). Given that the endocytic step of the BFA-sensitive PIN trafficking is dependent on clathrin (Adamowski et al., 2018; Narasimhan et al., 2021), this provides a functional link between Os12g01390, which encodes the CHC, and OsPIN3t.

To test whether the rice clathrin gene might respond to SA treatment, as its *Arabidopsis* homolog does (Du et al., 2013), and to find out whether it plays a role in rice root development, we analyzed the root phenotype of the T2 rice CHC mutants *chc11-cc* (#1, #2) and *chc12-cc* (#30; Figures 7d–i and S20). The results of this experiment showed that root lengths in the lines #1, #2 and #30 (Figure 7e,g,i) were not inhibited following treatment with 100 μM SA (Figure 7j) compared with the wild-type Nipponbare (Figure 7b,c). We also found that the root growth in lines #1, #2 and #30 (Figure 7m–r) was less sensitive to SA treatment (Figure 7n,p,r) than the control (Figure 7k,l) grown under gravity stimulation (Figure 7s). We then detected the effect of SA inhibition of endocytic trafficking on mutant lines #1, #2 and #30. The roots of mutant lines #1, #2 and #30 were co-treated with 100 μM SA, 25 μM BFA and 4 μM FM4-64 (Figure 8c–h); however, the sizes of BFA bodies in the mutant lines #1, #2 and #30 treated with SA (Figure 8d,f,h,i) were not inhibited compared with those in the wild-type (Figure 8a,b,i). Furthermore, when the rice lines expressing *35S::OsPIN3t-GFP* (Figure 8j–m) were treated with the CME inhibitor TyrA23(10 μM), BFA and SA, we found that the SA treatment did not inhibit the BFA-induced intracellular aggregation of OsPIN3t (Figure 8k,m,n) in the root epidermal cells compared with that in the control (Figure 8j,l,n).

The rice root growth and endocytic trafficking of *pin3t* mutant following TyrA23 treatment are insensitive to SA

To further check the involvement of OsPIN3t and clathrin in the regulation of rice root growth, we analyzed the expression levels of *OsPIN3t*, *CHC* (*LOC_Os11g01380* and *LOC_Os12g01390*) in the rice *chc11*-cc (#1, #2), *chc12-cc* (#30) and the *pin3t* mutant, respectively, following treatment with 100 μM SA. It showed that the levels of

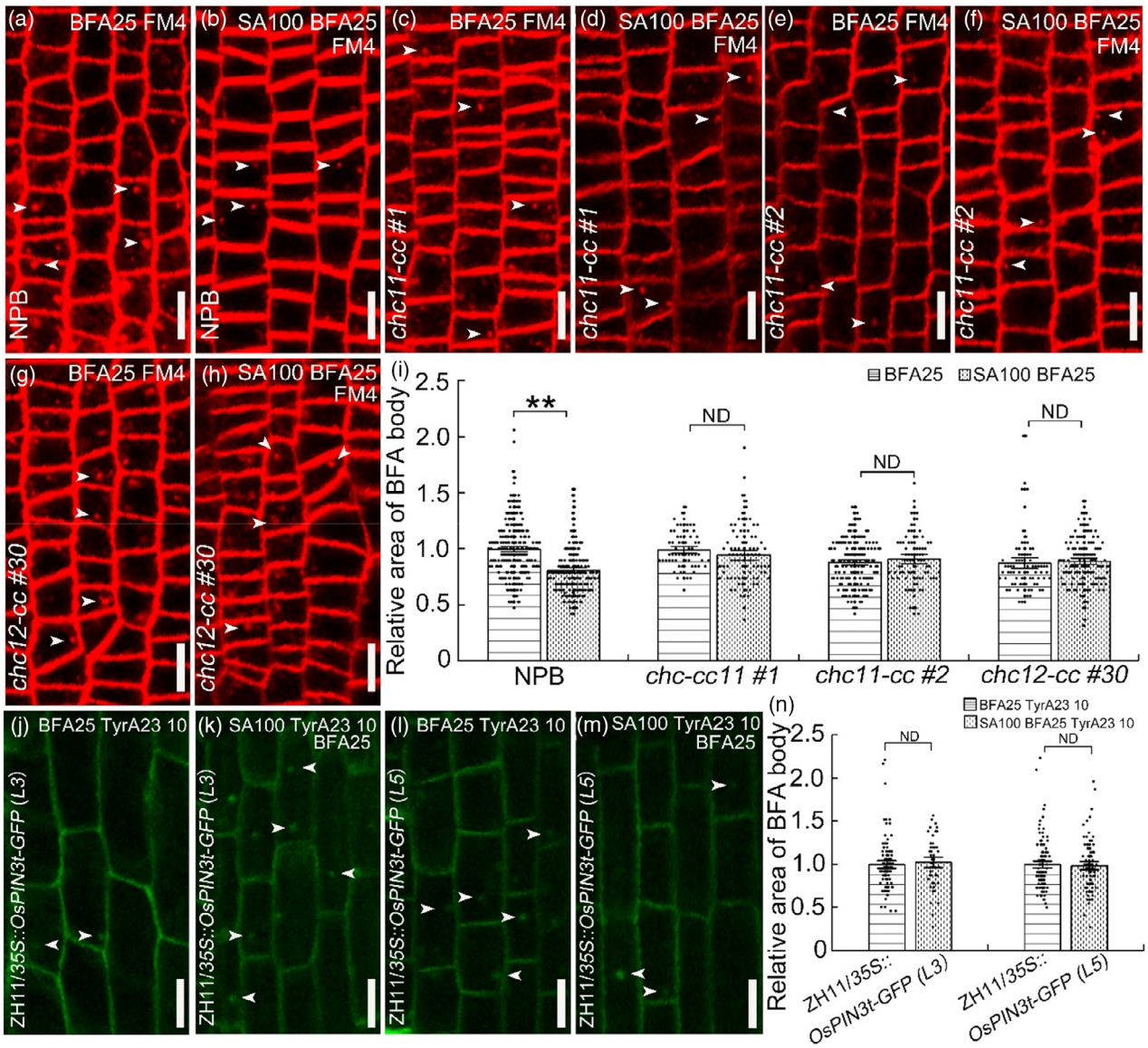

Figure 8. Salicylic acid (SA) inhibition of OsPIN3t endocytosis in rice epidermal cells was dependent on the clathrin heavy chain (CHC) gene.
The roots of 6-day-old seedlings of Nipponbare (a, b) and *chc11*-cc lines #1 (c, d), #2 (e, f), *chc12-cc* line #30 (g, h) were treated with 4 μM FM4-64 plus either 25 μM Brefeldin A (BFA) for 90 min (a, c, e, g) or with 4 μM FM4-64, 25 μM BFA and 100 μM SA (b, d, f, h). Quantification of the relative area of the BFA bodies (i) (NPB: $n_{BFA25} = 241$, $n_{SA100} = 199$, *chc11*-cc #1: $n_{DMSO} = 62$, $n_{SA100} = 83$, *chc11-cc* #2: $n_{DMSO} = 161$, $n_{SA100} = 78$, #30: $n_{DMSO} = 75$, $n_{SA100} = 125$) shown in images (a–h).
Roots of 14-day-old rice seedlings expressing *35S :: OsPIN3t-GFP* (j–m) were treated with 25 μM BFA and 10 μM TyrA23 for 90 min (j, l), or with 4 μM FM4-64, 25 μM BFA and with 100 μM SA (k, m). Quantification of the relative area of the internalized OsPIN3t-GFP proteins (n) (ZH11/*35S :: OsPIN3t-GFP* (*L3*): $n_{TyrA23\ 10BFA25} = 101$, $n_{TyrA23\ 10SA100BFA25} = 51$; ZH11/*35S :: OsPIN3t-GFP* (*L5*): $n_{TyrA23\ 10BFA25} = 118$, $n_{TyrA23\ 10SA100BFA25} = 90$) shown in images (j–m). Arrow heads indicate the BFA bodies. FM4, FM4-64; ND, no difference; NPB, Nipponbare; TyrA23, Tyrphostin A23; ZH11, Zhonghua 11. Data are means ± SD; $^{**}P < 0.01$ (Student's *t*-test). Scale bar: 10 μm.

LOC_Os11g01380 and *LOC_Os12g01390* were decreased in the wild-type ZH11 and *pin3t* mutant following 100 μM SA treatment compared with their respective controls (Figure S21a). However, the levels of *OsPIN3t* were decreased in the rice wild-type Nipponbare, but increased in the *chc11*-cc and *chc12-cc* mutants following 100 μM SA treatment compared with the control (Figure S21b). This suggests that the expression of *OsPIN3t* was negatively regulated by the *CHC* gene in rice roots following SA treatment. Next, we checked the root phenotype of the rice *pin3t* mutant treated with 10 μM TyrA23 and 100 μM SA. The root lengths of rice wild-type ZH11 (Figure 9c) and *pin3t* mutant (Figure 9f) co-treated with TyrA23 and SA were not significantly different (Figure 9g) from the control treated with TyrA23 alone (Figure 9a,b,d,e). Furthermore, the root bending in the wild-type rice ZH11 (Figure 9j) and the *pin3t*

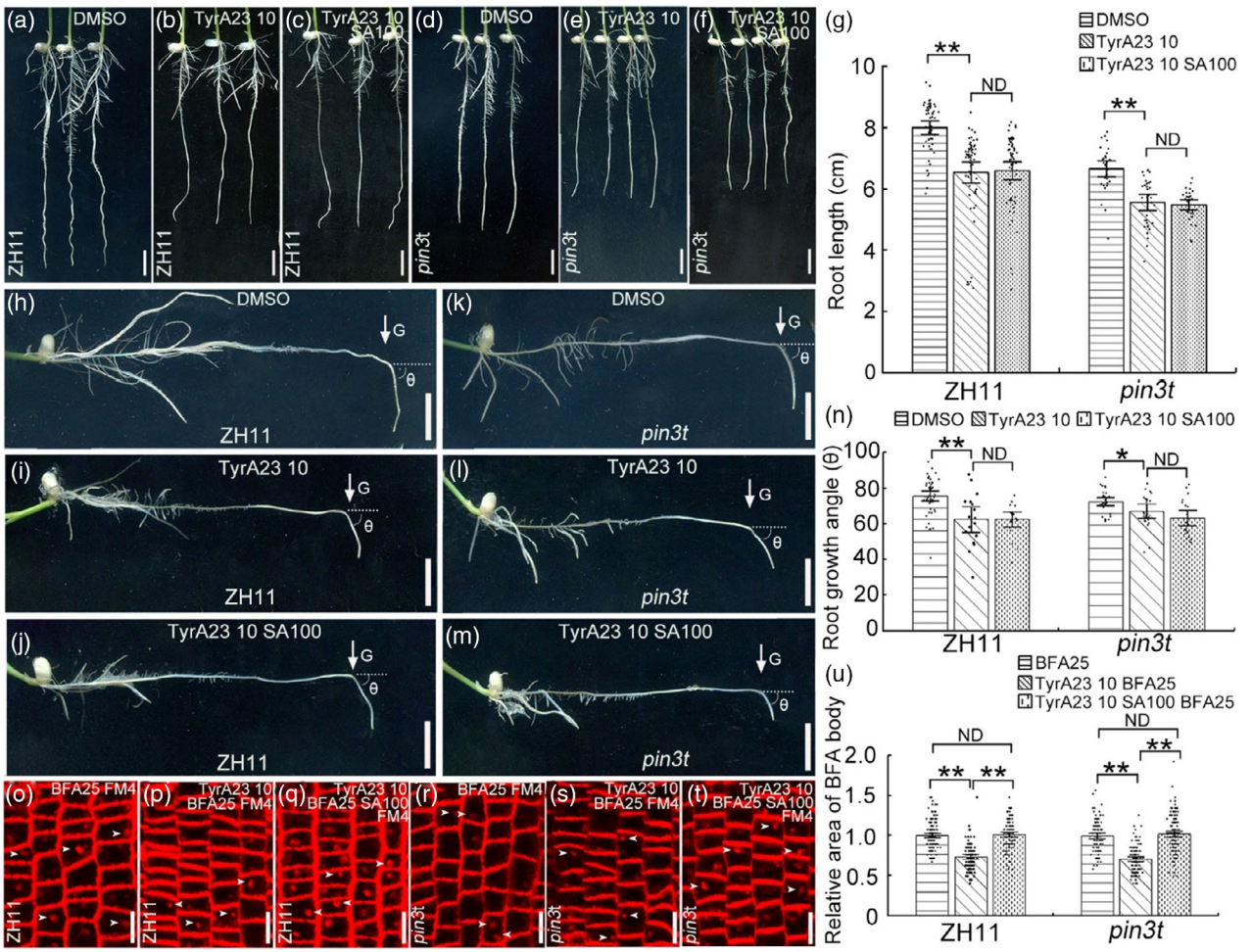

Figure 9. Salicylic acid (SA) did not inhibit root growth and endocytosis in the rice *pin3t* mutant following TyrA23 treatment.

Six-day-old seedlings of the rice line ZH11 (a–c) and the *pin3t* mutant (d–f) were grown on 1/2 Murashige and Skoog (MS) medium supplemented with either 100 μM SA plus 10 μM TyrA23 (c, f), 10 μM TyrA23 (b, e), or with an equivalent volume of dimethylsulfoxide (DMSO) (a, d) as a control. The primary root length was measured and quantified (g) (ZH11: $n_{DMSO} = 56$, $n_{TyrA23\ 10} = 63$, $n_{TyrA23\ 10/SA100} = 64$; *pin3t*: $n_{DMSO} = 32$, $n_{TyrA23\ 10} = 35$, $n_{TyrA23\ 10/SA100} = 33$) shown in images (a–f).

Six-day-old seedlings of rice ZH11 (h–j) and the *pin3t* mutant (k–m) were treated with either 10 μM TyrA23 (i, l), 10 μM TyrA23 plus 100 μM SA (j, m) or an equivalent volume of DMSO (h, k), and were grown on 1/2 MS medium with 18-h gravity stimulation. Quantification of the growth angles of the roots (n) shown in images (h–m) (ZH11: $n_{DMSO} = 53$, $n_{TyrA23\ 10} = 17$, $n_{TyrA23\ 10/SA100} = 19$; *pin3t*: $n_{DMSO} = 32$, $n_{TyrA23\ 10} = 23$, $n_{TyrA23\ 10/SA100} = 21$). The roots of 6-day-old ZH11 (o–q) and *pin3t* mutant (r–t) seedlings were treated with 4 μM FM4-64 and 25 μM Brefeldin A (BFA) (o, r) plus 10 μM TyrA23 (p, s) or cotreated with 100 μM SA (q, t) for 90 min. Quantification of the relative area of the BFA bodies (u) (ZH11: $n_{BFA25} = 166$, $n_{TyrA23\ 10/BFA25} = 113$, $n_{TyrA23\ 10/SA100BFA25} = 117$; *pin3t*: $n_{BFA25} = 117$, $n_{TyrA23\ 10/BFA25} = 137$, $n_{TyrA23\ 10/SA100/BFA25} = 165$) shown in images (o–t). Data are means ± SD; $*P < 0.05$, $**P < 0.01$ (Student's *t*-test). FM4, FM4-64; G, gravity; ND, no difference; TyrA23, Tyrphostin A23; ZH11, Zhonghua 11. Scale bar: 1 cm (images a–f, h–m); 10 μm (images o–t). Arrows indicate the direction of gravity. Arrow heads indicate the BFA bodies.

mutant (Figure 9m) treated with TyrA23 and grown under gravity stimulation was insensitive to SA treatment (Figure 9n) compared with the control (Figure 9h,i,k,l). We then detected the effect of SA inhibition of the endocytic trafficking in the *pin3t* mutant treated with TyrA23. The roots of the wild-type ZH11 (Figure 9q) and the *pin3t* mutant (Figure 9t) were co-treated with 100 μM SA, 10 μM TyrA23, 25 μM BFA and 4 μM FM4-64. Compared with the controls treated with 25 μM BFA and 4 μM FM4-64 (Figure 9o,r) and 10 μM TyrA23, 25 μM BFA and 4 μM FM4-64 (Figure 9p,s) separately, there was no SA-mediated inhibition of the endocytic trafficking in the wild-type ZH11 (Figure 9q,u) or the *pin3t* mutant (Figure 9t,u). These above data suggest that the clathrin-mediated endocytic trafficking processes involved in the SA regulation of rice root growth are independent of the *OsPIN3t* gene.

DISCUSSION

Salicylic acid is known to play several important roles in plant development. In this study, we found that SA affects rice root growth through a convergence of non-SA signaling and transcriptional mechanisms. The key component

of this regulation is the OsPIN3t mediator of polar auxin transport, whose endocytic trafficking depends on the coat protein clathrin. Transcriptome analysis revealed that *OsPIN3t* and *clathrin* were located in the same GRN responding to SA. However, SA affects root growth via a non-canonical mechanism, which is independent of the established OsNPR1 receptor, and depends on the CHC and OsPIN3t. SA interferes with auxin transport and the endocytic trafficking of OsPIN3t in a CME manner; however, root growth and endocytic trafficking in the *pin3t* under TyrA23 treatment are insensitive to SA, implying that SA affects root growth via a complicated GRN mediated by the clathrin and OsPIN3t.

Rice and *Arabidopsis* have different root development patterns. Nonetheless, SA can inhibit the endocytic trafficking in both *Arabidopsis* (Du et al., 2013) and rice (Figure 3), implying that the mechanism of SA inhibited endocytosis may be conserved in both dicotyledonous and monocotyledonous plants. Moreover, SA inhibition of root growth through the disturbance of OsPIN3t-regulated polar auxin transport (Figure 6) was independent of the canonical SA signaling pathway (Figure 2). Previous research shows that overexpression of *OsNPR1* decreases the extent of rice root system, and is also associated with lower IAA levels and alteration of the *OsGH3.8*-regulated auxin distribution (Li et al., 2016). This suggests that SA and OsNPR1 utilize two different pathways to regulate auxin-mediated root development.

In *Arabidopsis*, the polar auxin transport mediated by the auxin efflux carrier family proteins PIN1 and PIN2 (Adamowski & Friml, 2015; Friml, 2022) is known to play an important role in the interference of SA with root growth (Du et al., 2013; Zhao et al., 2015). SA is also known to affect the expression of *PIN1*, *PIN2*, *PIN3*, *PIN4* and *PIN7* (Armengot et al., 2014; Pasternak et al., 2019). In this study, SA inhibition of rice root growth was dependent on OsPIN3t-regulated polar auxin transport (Figure 6). The OsPIN3t localizes to the plasma membrane of rice root epidermal cells and vascular bundles (Zhang et al., 2012). However, AtPIN3 symmetrically localizes at the plasma membrane of columella cells (Friml et al., 2002), and clathrin is known to mediate the endocytosis of both AtPIN3 (Rakusova et al., 2016) and OsPIN3t (Figures 3p–t and 8j–n). The SA-inhibited CME of OsPIN3t (Figure 8) and the differential *PIN3* expression patterns observed in rice and *Arabidopsis* suggest that SA-inhibited growth of rice roots may occur via clathrin-associated inhibition of auxin flux in the epidermal cells and vascular bundles.

Salicylic acid regulation of root development involves different cellular processes including auxin distribution (Du et al., 2013; Ke et al., 2021). In this study, transcriptome analysis revealed a central role for *OsPIN3t* in the network of gene expression (Figure 5). The function of OsPIN3t is directly or indirectly involved in the regulation of many physiological processes, including the development of roots, shoots, inflorescences, panicles, tillers, grains and leaves (Figure 7a). It is plausible that SA affects auxin transport via the action of OsPIN3t, in order to keep a balance between root growth and different physiological activities. Meanwhile, clathrin is involved in the endocytosis pathway in plant development (Du et al., 2013). An *Arabidopsis* clathrin defective mutant (Du et al., 2013) and a rice clathrin mutant (Figure 7k–s) were found to be insensitive to SA treatment on root gravitropic stimulation. This suggests that the CME has a conserved role in the SA inhibition of root development in dicotyledons and monocotyledons. However, the root growth and endocytic trafficking mediated by the TyrA23 were independent of the *OsPIN3t* gene under SA treatment (Figure 9), and the *CHC* gene negatively regulates the expression of *OsPIN3t* gene (Figure S21b). It suggests that the GRN mediated by the *OsPIN3t* and *CHC* genes regulates rice root growth through the regulation of auxin transport under SA treatment. Further elucidation of the network components of the pathway mediated by the *OsPIN3t* and *CHC* genes will provide us with an insight into the effects of SA on root development.

EXPERIMENTAL PROCEDURES

Plant material and growth conditions

The rice plants used in this study were from the transgenic lines NB-7B-70 (in a NB-61-WT background), *NahG* (in a Nipponbare background; Yang et al., 2004), *OsNPR1*-RNAi (in a TP309 background; Yuan et al., 2007), *OsPIN3t*-RNAi (in a ZH11 background; Zhang et al., 2012) and *35S :: OsPIN3t-GFP* line (in a Zhonghua 11 background; Zhang et al., 2012). The rice *npr1* (in a ZH11 background) and *pin3t* (in a ZH11 background) mutants were obtained from Biogle (Hangzhou Biogle Co., Ltd, Hangzhou, China). The seeds of rice varieties, including LTH, Nipponbare, ZH11 and different transgenic lines and mutants, were grown on 1/2 Murashige and Skoog (MS, M5519; Sigma-Aldrich Trading Co., Ltd, Shanghai, China) medium without supplementation of hormones or sugar in vertically oriented plates at 28°C in darkness for 2 days, and then grown in 12-h light conditions for 4 days. To induce germination of rice *NahG*, the seeds of *NahG* were grown on 1/2 MS medium at 28°C in darkness for 3 days, and then in 12-h light conditions for 4 days. To obtain high expression levels of transgenes, 6-day-old seedlings of transgenic rice Nipponbare expressing *pOsPIN1b :: OsPIN1b-GFP*, *pOsPIN2 :: OsPIN2-GFP* and *35S :: OsPIN3t-GFP* were grown in water conditions for 8 days under 12-h light conditions.

Drug treatments and confocal microscopy observation

To observe subcellular endocytosis, root tips from 6-day-old seedlings were incubated for the indicated times in a sterilized water solution supplemented with appropriate volumes of 4 μM FM4-64 (ThermoFisher Scientific Inc, Waltham, United States), 100 μM SA (Sigma-AldrichTrading Co., Ltd), 25 μM BFA (Thermo Fisher Scientific Inc, Waltham, MA, USA), 10 μM TyrA23, 50 μM CHX (Sigma-AldrichTrading Co., Ltd) and 50 μM MG132 (Sigma-AldrichTrading Co., Ltd) dissolved with DMSO, as described previously (Du et al., 2013). Confocal images were obtained using a Leica spectral confocal microscope (Leica SP5; Leica Microsystems, Wetzlar, Germany). The relative area of the internalized proteins (BFA

bodies) and the relative fluorescence intensity at the plasma membrane were measured using ImageJ 1.41 software (Kitakura et al., 2011) as described previously (Du et al., 2013).

Growth of rice seedlings under gravity stimulation and treatment with SA

To observe root lengths of rice seedlings treated with SA, rice seeds were surface-sterilized with 70% ethanol for 90 sec and 2% sodium hypochlorite for 15 min, washed with sterilized water five times and cultured on 1/2 MS medium grown in darkness for 2 days. Rice seedlings were then transferred to 1/2 MS medium supplemented with 100 μM SA and grown for 4 days under 12-h light conditions. The gravity stimulation experiment was conducted as described previously (Du et al., 2013) with a minor modification. Briefly, the rice seedlings were grown for 6 days on 1/2 MS medium, then transferred to 1/2 MS medium supplemented with 100 μM SA, after which the plates were turned 90° and grown under gravity stimulation for 18 or 120 h under 12-h light conditions.

Rice root transcriptome analysis

RNA sequencing of the rice line LTH was performed using six samples, including three samples treated with DMSO, and three samples were treated with SA. Six-day-old rice LTH seedlings were grown on 1/2 MS medium supplemented with 2 mM SA for 4 days, and with other seedlings treated with DMSO acting as a control. The isolation, measurement, quantification of total mRNA, construction of the RNA library and the paired-end sequencing of sample cDNA from the LTH roots were carried out as described in a previous report (Han et al., 2020), and were performed by Biomarker Technologies (Beijing, China). The transcriptome data from the rice roots were submitted to the Genome Sequence Archive (GSA) public database (http://gsa.big.ac.cn; accession no. CRA002673). Using HISAT2 software, the clean reads were aligned to the reference Nipponbare genome (MSU Rice Genome Annotation Project release 7). Subsequently, the mapped reads were assembled to generate unigenes in the software StringTie. Expression levels of unigenes were analyzed using DEseq2 (Love et al., 2014), and assessment of biological replication was performed using Pearson's Correlation Coefficient (Formula 1).

$$R_{x,y} = \frac{\sum_{i=1}^{n}(X_i-\overline{X})(Y_i-\overline{Y})}{\sqrt{\sum_{i=1}^{n}(X_i-\overline{X})^2}\sqrt{\sum_{i=1}^{n}(Y_i-\overline{Y})^2}} \qquad \text{(Formula 1)}$$

In the above formula, n is the number of unigenes, X_i and Y_i are expression levels of unigene i in samples X and Y, $\overline{X}$ and $\overline{Y}$ are average expression levels of unigenes in different samples. The Pearson's Correlation Coefficient value $R_{x,y}$ ranges from −1 to 1, and a value close to 1 implies that the datasets are faithful replicates.

Construction of the GRN

A GRN was constructed using RicNetDB by combining the results of the DEGs analysis and the regulatory relationship pairs between them and directly regulated genes (Lee et al., 2011; Liu et al., 2013). DEGs with MSU_IDs were loaded into RiceNetDB, and a regulatory relationship pair was maintained when the log likelihood score of two genes with an association was more than 1.0. The GRN was visualized in Cytoscape (version 3.7.2). To find the potentially important nodes in the network, a plugin cytoHubba was used to search the hub genes, which were defined as genes with high degrees of connectivity (here we use a threshold of more than 200) and are more likely to be essential (Chin et al., 2014). The sub-GRN of given genes was constructed using breadth-first search.

Microscope observation of rice root subcellular structure

The root tips of 6-day-old Nipponbare rice seedlings were treated with 100 μM SA dissolved in DMSO or with an equivalent volume of DMSO (acting as a control) as described previously (Du et al., 2013). For observation of the subcellular structure of the root tips, we used a transmission electron microscope (TEM), and followed standard protocol for sample preparation. The meristem region of rice primary roots was cut into small pieces (1 × 1 mm), fixed with glutaric dialdehyde and osmium (VIII) oxide twice and, after dehydration with ethyl alcohol, was embedded in a resin containing the agents Dow epoxy resin (DER) 736, 1-nonenylsuccinic anhydride, aliphatic epoxy resin ERL-4221 and dimethylaminoethanol. The samples were then sectioned to a thickness of 70 nm in a LEICA EM UC7 ultramicrotome and were stained with uranyl acetate (Zhong Jing Ke Yi Technology Co., Ltd, Beijing, China) for 15 min, and alkaline lead citrate, containing trisodium citrate dehydrates, lead nitrate and sodium hydroxide, for 5 min. The specimens were then examined using a FEI TECNAI SPIRIT G2 TEM under a voltage of 80 kV and a current of 27 A. For observation of the BFA bodies, root meristem regions were incubated in sterilized water solution supplemented with 25 μM BFA for 90 min as described previously (Du et al., 2013), and were then subjected to the above procedure for examination under the TEM.

Analysis of rice root phenotype

The software ImageJ 1.41 was used for the measurement of the root growth angle, root length, fluorescence intensities and relative areas of BFA bodies. All images were processed in the Photoshop software.

AUTHOR CONTRIBUTIONS

YD initiated the project. YD, C. Liu. and Z. Zhang supervised the project. YD, JF and XH designed the experiments. LJ, BY, LW and X. Zhang performed the majority of the experiments, and analyzed and prepared the figures. QF, YZ, YC, RZ, XL, WH, JZ, KL, SZ, LH, X. Zhou, C. Luo and HZ performed additional experiments. YD, C. Liu, Z. Zhang, XH, Z. Zhu, HH and JY analyzed the data. YD, C. Liu., Z. Zhang and JF wrote and revised the paper with input from all authors.

ACKNOWLEDGEMENTS

The authors thank Professor Jianqiang Wu (Kunming Institute of Botany, Chinese Academy of Sciences) for support with phytohormone measurement. Thanks also go to Professor Pieter. B. F. Ouwerkerk (Leiden University) and Professor Jean-Benoit Morel (Plant Health Institute of Montpellier) for provision of the rice lines NB-7B-70 and NB-7B-76 and wild-type NB-61-WT, Professor Zuhua He (Chinese Academy of Sciences) for provision of the rice *OsNPR1*-RNAi mutant, and Professor Yinong Yang (The Pennsylvania State University) for provision of the rice line *NahG*. This work was supported by grants from the National Natural Science Foundation of China (Grant Nos. 32260085, 31460453, 31660501, 31860064, 31970609, 31801792 and 31960554), the Key Projects of the Applied Basic Research Plan

of Yunnan Province (202301AS070082), the Major Special Program for Scientific Research, Education Department of Yunnan Province (Grant No. ZD2015005), the Start-up fund from Xishuangbanna Tropical Botanical Garden, and 'Top Talents Program in Science and Technology' from Yunnan Province, the SRF for ROCS, SEM (Grant No. [2013] 1792), and the Major Science and Technology Project in Yunnan Province (202102AE090042 and 202202AE090036); and the young and middle-aged academic and technical leaders reserve talent program in Yunnan Province (202205AC160076).

CONFLICT OF INTEREST

The authors declare no competing interests.

DATA AVAILABILITY STATEMENT

The data that support the findings of this study are available from the corresponding author upon reasonable request.

SUPPORTING INFORMATION

Additional Supporting Information may be found in the online version of this article.

Additional File S1. Summary of domains in the auxin transport proteins PIN1, PIN2 and PIN3.

Additional File S2. Quality of sequencing.

Additional File S3. All unigenes.

Additional File S4. Expression levels of DEGs treated with DMSO and salicylic acid.

Additional File S5. Summary of relevant literature on differential genes.

Additional File S6. GO enrichment analysis up.

Additional File S7. GO enrichment analysis down.

Additional File S8. Gene regulatory network.

Additional File S9. 30 hub genes in the gene regulatory network.

Figure S1. SA content in the roots of different rice varieties.

Figure S2. SA treatment inhibits roots growth in rice.

Figure S3. Gene expression levels of *OsNPR1* in the rice line *OsNPR1*-RNAi.

Figure S4. Sequence profiles and gene expression levels of the *OsNPR1* gene in rice wild-type Zhonghua 11 and *npr1* mutant.

Figure S5. SA inhibited root growth of rice *npr1* mutant.

Figure S6. SA treatment disturbed auxin transport of rice roots grown under gravity stimulation.

Figure S7. SA treatment inhibition of endocytosis in root epidermal cells was independent of protein degradation.

Figure S8. Sequence alignments of the auxin transporters PIN1, PIN2 and PIN3 in rice and *Arabidopsis*.

Figure S9. SA treatment did not disturb the ultrastructures of organelles or vesicle compartments in rice root epidermal cells.

Figure S10. Biological replicates correlation assessment and analysis of unigenes.

Figure S11. Functional enrichment analysis of GO terms.

Figure S12. Functional enrichment analysis of KEGG pathways.

Figure S13. Heat map and PCR detection of rice unigenes.

Figure S14. Gene regulatory network of rice seedlings treated with SA.

Figure S15. Gene expression levels of *OsPIN3t* in rice roots.

Figure S16. Sequence profiles of the *OsPIN3t* gene in the wild-type rice Zhonghua 11 and the pin3t mutant.

Figure S17. The root growth in the rice *pin3t* mutant following treatment with SA.

Figure S18. Gene expression levels of *OsPIN3t* in the rice line *OsPIN3t*-RNAi.

Figure S19. Root growth in the rice *OsPIN3t*-RNAi line was insensitive to SA treatment.

Figure S20. Sequence profiles of the *CHC* gene in the wild-type rice Nipponbare and two *chc* knockout mutants.

Figure S21. Gene expression levels of *CHC* and *OsPIN3t* in the rice *pin3t* and clathrin heavy chain mutants.

Table S1 Sequences of gene-specific primers

Table S2 Sequences of gene-specific primers for transcriptome data and RT-qPCR detection

Methods S1. Construction of the OsPIN1b and OsPIN2 transgenic rice lines.

Methods S2. Construction of the clathrin heavy chain, OsPIN3t and OsNPR1 knockout mutants.

Methods S3. Measurement of the phytohormones SA and IAA.

Methods S4. RNA isolation and cDNA synthesis.

Methods S5. Real-time PCR analysis.

Methods S6. Function annotation of all unigenes.

Methods S7. Identification of differentially expressed unigenes.

Methods S8. Functional enrichment analysis of differentially expressed unigenes.

Methods S9. Sequences alignment and domain searching.

REFERENCES

Adamowski, M. & **Friml, J.** (2015) PIN-dependent auxin transport: action, regulation, and evolution. *Plant Cell*, **27**, 20–32. Available from: https://doi.org/10.1105/tpc.114.134874

Adamowski, M., **Narasimhan, M.**, **Kania, U.**, **Glanc, M.**, **De Jaeger, G.** & **Friml, J.** (2018) A functional study of AUXILIN-LIKE1 and 2, two putative clathrin uncoating factors in *Arabidopsis*. *Plant Cell*, **30**, 700–716. Available from: https://doi.org/10.1105/tpc.17.00785

Armengot, L., **Marques-Bueno, M.M.**, **Soria-Garcia, A.**, **Muller, M.**, **Munne-Bosch, S.** & **Martinez, M.C.** (2014) Functional interplay between protein kinase CK2 and salicylic acid sustains PIN transcriptional expression and root development. *The Plant Journal*, **78**, 411–423. Available from: https://doi.org/10.1111/tpj.12481

Chen, X., **Irani, N.G.** & **Friml, J.** (2011) Clathrin-mediated endocytosis: the gateway into plant cells. *Current Opinion in Plant Biology*, **14**, 674–682. Available from: https://doi.org/10.1016/j.pbi.2011.08.006

Chen, Y., **Fan, X.**, **Song, W.**, **Zhang, Y.** & **Xu, G.** (2012) Over-expression of OsPIN2 leads to increased tiller numbers, angle and shorter plant height through suppression of OsLAZY1. *Plant Biotechnology Journal*, **10**, 139–149. Available from: https://doi.org/10.1111/j.1467-7652.2011.00637.x

Chin, C.H., **Chen, S.H.**, **Wu, H.H.**, **Ho, C.W.**, **Ko, M.T.** & **Lin, C.Y.** (2014) CytoHubba: identifying hub objects and sub-networks from complex interactome. *BMC Systems Biology*, **8**(Suppl 4), S11. Available from: https://doi.org/10.1186/1752-0509-8-S4-S11

Ding, Y., **Sun, T.**, **Ao, K.**, **Peng, Y.**, **Zhang, Y.**, **Li, X.** ***et al.*** (2018) Opposite roles of salicylic acid receptors NPR1 and NPR3/NPR4 in transcriptional regulation of plant immunity. *Cell*, **173**, 1454–1467.e15. Available from: https://doi.org/10.1016/j.cell.2018.03.044

Du, Y., **Tejos, R.**, **Beck, M.**, **Himschoot, E.**, **Li, H.**, **Robatzek, S.** ***et al.*** (2013) Salicylic acid interferes with clathrin-mediated endocytic protein trafficking. *Proceedings of the National Academy of Sciences of the United States of America*, **110**, 7946–7951. Available from: https://doi.org/10.1073/pnas.1220205110

Feng, Z., **Wu, C.**, **Wang, C.**, **Roh, J.**, **Zhang, L.**, **Chen, J.** ***et al.*** (2016) SLG controls grain size and leaf angle by modulating brassinosteroid homeostasis in rice. *Journal of Experimental Botany*, **67**, 4241–4253. Available from: https://doi.org/10.1093/jxb/erw204

Friml, J. (2022) Fourteen stations of auxin. *Cold Spring Harbor Perspectives in Biology*, **14**(5), a039859. Available from: https://doi.org/10.1101/cshperspect.a039859

Friml, J., Wisniewska, J., Benkova, E., Mendgen, K. & **Palme, K.** (2002) Lateral relocation of auxin efflux regulator PIN3 mediates tropism in *Arabidopsis*. *Nature*, **415**, 806–809. Available from: https://doi.org/10.1038/415806a

Garcia-Sanchez, S., Bernales, I. & **Cristobal, S.** (2015) Early response to nanoparticles in the *Arabidopsis* transcriptome compromises plant defence and root-hair development through salicylic acid signalling. *BMC Genomics*, **16**, 341. Available from: https://doi.org/10.1186/s12864-015-1530-4

Geldner, N., Friml, J., Stierhof, Y.D., Jurgens, G. & **Palme, K.** (2001) Auxin transport inhibitors block PIN1 cycling and vesicle trafficking. *Nature*, **413**, 425–428. Available from: https://doi.org/10.1038/35096571

Han, L., Zhou, X., Zhao, Y., Zhu, S., Wu, L., He, Y. *et al.* (2020) Colonization of endophyte *Acremonium* sp. D212 in *Panax notoginseng* and rice mediated by auxin and jasmonic acid. *Journal of Integrative Plant Biology*, **62**, 1433–1451. Available from: https://doi.org/10.1111/jipb.12905

Inahashi, H., Shelley, I.J., Yamauchi, T., Nishiuchi, S., Takahashi-Nosaka, M., Matsunami, M. *et al.* (2018) OsPIN2, which encodes a member of the auxin efflux carrier proteins, is involved in root elongation growth and lateral root formation patterns via the regulation of auxin distribution in rice. *Physiologia Plantarum*, **164**, 216–225. Available from: https://doi.org/10.1111/ppl.12707

Jelinkova, A., Malinska, K., Simon, S., Kleine-Vehn, J., Parezova, M., Pejchar, P. *et al.* (2010) Probing plant membranes with FM dyes: tracking, dragging or blocking? *The Plant Journal*, **61**, 883–892. Available from: https://doi.org/10.1111/j.1365-313X.2009.04102.x

Kang, Z., Qin, T. & **Zhao, Z.** (2019) Overexpression of the zinc finger protein gene OsZFP350 improves root development by increasing resistance to abiotic stress in rice. *Acta Biochimica Polonica*, **66**, 183–190. Available from: https://doi.org/10.18388/abp.2018_2765

Ke, M., Ma, Z., Wang, D., Sun, Y., Wen, C., Huang, D. *et al.* (2021) Salicylic acid regulates PIN2 auxin transporter hyperclustering and root gravitropic growth via Remorin-dependent lipid nanodomain organisation in *Arabidopsis thaliana*. *The New Phytologist*, **229**, 963–978. Available from: https://doi.org/10.1111/nph.16915

Kim, T.H., Kunz, H.H., Bhattacharjee, S., Hauser, F., Park, J., Engineer, C. *et al.* (2012) Natural variation in small molecule-induced TIR-NB-LRR signaling induces root growth arrest via EDS1- and PAD4-complexed R protein VICTR in *Arabidopsis*. *Plant Cell*, **24**, 5177–5192. Available from: https://doi.org/10.1105/tpc.112.107235

Kitakura, S., Vanneste, S., Robert, S., Lofke, C., Teichmann, T., Tanaka, H. *et al.* (2011) Clathrin mediates endocytosis and polar distribution of PIN auxin transporters in *Arabidopsis*. *Plant Cell*, **23**, 1920–1931. Available from: https://doi.org/10.1105/tpc.111.083030

Lee, I., Seo, Y.S., Coltrane, D., Hwang, S., Oh, T., Marcotte, E.M. *et al.* (2011) Genetic dissection of the biotic stress response using a genome-scale gene network for rice. *Proceedings of the National Academy of Sciences of the United States of America*, **108**, 18548–18553. Available from: https://doi.org/10.1073/pnas.1110384108

Li, X., Yang, D.L., Sun, L., Li, Q., Mao, B. & **He, Z.** (2016) The systemic acquired resistance regulator OsNPR1 attenuates growth by repressing auxin signaling through promoting IAA-amido synthase expression. *Plant Physiology*, **172**, 546–558. Available from: https://doi.org/10.1104/pp.16.00129

Li, Y., Zhu, J., Wu, L., Shao, Y., Wu, Y. & **Mao, C.** (2019) Functional divergence of PIN1 paralogous genes in rice. *Plant & Cell Physiology*, **60**, 2720–2732. Available from: https://doi.org/10.1093/pcp/pcz159

Liu, L., Mei, Q., Yu, Z., Sun, T., Zhang, Z. & **Chen, M.** (2013) An integrative bioinformatics framework for genome-scale multiple level network reconstruction of rice. *Journal of Integrative Bioinformatics*, **10**, 223. Available from: https://doi.org/10.2390/biecoll-jib-2013-223

Liu, L., Tong, H., Xiao, Y., Che, R., Xu, F., Hu, B. *et al.* (2015) Activation of big Grain1 significantly improves grain size by regulating auxin transport in rice. *Proceedings of the National Academy of Sciences of the United States of America*, **112**, 11102–11107. Available from: https://doi.org/10.1073/pnas.1512748112

Love, M.I., Huber, W. & **Anders, S.** (2014) Moderated estimation of fold change and dispersion for RNA-seq data with DESeq2. *Genome Biology*, **15**, 550. Available from: https://doi.org/10.1186/s13059-014-0550-8

Narasimhan, M., Gallei, M., Tan, S., Johnson, A., Verstraeten, I., Li, L. *et al.* (2021) Systematic analysis of specific and nonspecific auxin effects on endocytosis and trafficking. *Plant Physiology*, **186**, 1122–1142. Available from: https://doi.org/10.1093/plphys/kiab134

Pasternak, T., Groot, E.P., Kazantsev, F.V., Teale, W., Omelyanchuk, N., Kovrizhnykh, V. *et al.* (2019) Salicylic acid affects root meristem patterning via auxin distribution in a concentration-dependent manner. *Plant Physiology*, **180**, 1725–1739. Available from: https://doi.org/10.1104/pp.19.00130

Rakusova, H., Abbas, M., Han, H., Song, S., Robert, H.S. & **Friml, J.** (2016) Termination of shoot gravitropic responses by auxin feedback on PIN3 polarity. *Current Biology*, **26**, 3026–3032. Available from: https://doi.org/10.1016/j.cub.2016.08.067

Sun, H., Guo, X., Xu, F., Wu, D., Zhang, X., Lou, M. *et al.* (2019) Overexpression of OsPIN2 regulates root growth and formation in response to phosphate deficiency in rice. *International Journal of Molecular Sciences*, **20**, 5144. Available from: https://doi.org/10.3390/ijms20205144

Tan, S., Abas, M., Verstraeten, I., Glanc, M., Molnar, G., Hajny, J. *et al.* (2020) Salicylic acid targets protein phosphatase 2A to attenuate growth in plants. *Current Biology*, **30**, 381–395.e8. Available from: https://doi.org/10.1016/j.cub.2019.11.058

Wang, C., Hu, T., Yan, X., Meng, T., Wang, Y., Wang, Q. *et al.* (2016) Differential regulation of clathrin and its adaptor proteins during membrane recruitment for endocytosis. *Plant Physiology*, **171**, 215–229. Available from: https://doi.org/10.1104/pp.15.01716

Wang, J.R., Hu, H., Wang, G.H., Li, J., Chen, J.Y. & **Wu, P.** (2009) Expression of PIN genes in rice (*Oryza sativa* L.): tissue specificity and regulation by hormones. *Molecular Plant*, **2**, 823–831. Available from: https://doi.org/10.1093/mp/ssp023

Wang, L., Guo, M., Li, Y., Ruan, W., Mo, X., Wu, Z. *et al.* (2018) LARGE ROOT ANGLE1, encoding OsPIN2, is involved in root system architecture in rice. *Journal of Experimental Botany*, **69**, 385–397. Available from: https://doi.org/10.1093/jxb/erx427

Wu, D., Shen, H., Yokawa, K. & **Baluška, F.** (2015) Overexpressing OsPIN2 enhances aluminium internalization by elevating vesicular trafficking in rice root apex. *Journal of Experimental Botany*, **66**(21), 6791–6801. Available from: https://doi.org/10.1093/jxb/erv385

Wu, Y., Zhang, D., Chu, J.Y., Boyle, P., Wang, Y., Brindle, I.D. *et al.* (2012) The *Arabidopsis* NPR1 protein is a receptor for the plant defense hormone salicylic acid. *Cell Reports*, **1**, 639–647. Available from: https://doi.org/10.1016/j.celrep.2012.05.008

Xu, C., Liu, Y., Li, Y., Xu, X., Xu, C., Li, X. *et al.* (2015) Differential expression of GS5 regulates grain size in rice. *Journal of Experimental Botany*, **66**, 2611–2623. Available from: https://doi.org/10.1093/jxb/erv058

Xu, M., Zhu, L., Shou, H. & **Wu, P.** (2005) A PIN1 family gene, OsPIN1, involved in auxin-dependent adventitious root emergence and tillering in rice. *Plant & Cell Physiology*, **46**, 1674–1681. Available from: https://doi.org/10.1093/pcp/pci183

Yan, S. & **Dong, X.** (2014) Perception of the plant immune signal salicylic acid. *Current Opinion in Plant Biology*, **20**, 64–68. Available from: https://doi.org/10.1016/j.pbi.2014.04.006

Yang, L., Zhao, M., Sha, G., Sun, Q., Gong, Q., Yang, Q. *et al.* (2022) The genome of the rice variety LTH provides insight into its universal susceptibility mechanism to worldwide rice blast fungal strains. *Computational and Structural Biotechnology Journal*, **20**, 1012–1026. Available from: https://doi.org/10.1016/j.csbj.2022.01.030

Yang, S.Q., Li, W.Q., Miao, H., Gan, P.F., Qiao, L., Chang, Y.L. *et al.* (2016) REL2, a gene encoding an unknown function protein which contains DUF630 and DUF632 domains controls leaf rolling in rice. *Rice (New York, N.Y.)*, **9**, 37. Available from: https://doi.org/10.1186/s12284-016-0105-6

Yang, X.Y., Zeng, Z.H., Yan, J.Y., Fan, W., Bian, H.W., Zhu, M.Y. *et al.* (2013) Association of specific pectin methylesterases with Al-induced root elongation inhibition in rice. *Physiologia Plantarum*, **148**, 502–511. Available from: https://doi.org/10.1111/ppl.12005

Yang, Y., Qi, M. & **Mei, C.** (2004) Endogenous salicylic acid protects rice plants from oxidative damage caused by aging as well as biotic and abiotic stress. *The Plant Journal*, **40**, 909–919. Available from: https://doi.org/10.1111/j.1365-313X.2004.02267.x

Yuan, Y., Zhong, S., Li, Q., Zhu, Z., Lou, Y., Wang, L. *et al.* (2007) Functional analysis of rice NPR1-like genes reveals that OsNPR1/NH1 is the rice

orthologue conferring disease resistance with enhanced herbivore susceptibility. *Plant Biotechnology Journal*, **5**, 313–324. Available from: https://doi.org/10.1111/j.1467-7652.2007.00243.x

Zhang, Q., **Li, J.**, **Zhang, W.**, **Yan, S.**, **Wang, R.**, **Zhao, J.** ***et al.*** (2012) The putative auxin efflux carrier OsPIN3t is involved in the drought stress response and drought tolerance. *The Plant Journal*, **72**, 805–816. Available from: https://doi.org/10.1111/j.1365-313X.2012.05121.x

Zhao, X., **Wang, J.**, **Yuan, J.**, **Wang, X.L.**, **Zhao, Q.P.**, **Kong, P.T.** ***et al.*** (2015) NITRIC OXIDE-ASSOCIATED PROTEIN1 (AtNOA1) is essential for salicylic acid-induced root waving in *Arabidopsis thaliana*. *The New Phytologist*, **207**, 211–224. Available from: https://doi.org/10.1111/nph.13327

Zhao, Y., **Wu, L.**, **Fu, Q.**, **Wang, D.**, **Li, J.**, **Yao, B.** ***et al.*** (2021) INDITTO2 transposon conveys auxin-mediated DRO1 transcription for rice drought avoidance. *Plant, Cell & Environment*, **44**, 1846–1857. Available from: https://doi.org/10.1111/pce.14029

Zhou, J.M. & **Zhang, Y.** (2020) Plant immunity: danger perception and signaling. *Cell*, **181**, 978–989. Available from: https://doi.org/10.1016/j.cell.2020.04.028